



ANALYSIS OF QUASI-ISOMETRIC POLYGONAL BUCKLING SHAPES OF SPHERICAL SHELLS

PhD dissertation

*A dissertation submitted to the
Budapest University of Technology and Economics
in partial fulfilment of the requirements for the degree of
Doctor of Philosophy*

Dániel Vető

Supervisor:

István Sajtos

Budapest University of Technology and Economics
Department of Mechanics, Materials and Structures

2016

Table of contents

Brief summary	4
Brief summary in Hungarian – Rövid összefoglalás	5
1. Introduction	6
1.1. Background of the research, motivation	6
1.2. The goal of the research	12
1.3. Basic assumptions	13
2. Analysis of axisymmetric buckling shapes	14
2.1. Inextensional (isometric) deformations	14
2.2. Energy method	19
2.3. Axisymmetric buckling shapes, concentrated force – Pogorelov’s results	22
2.4. Axisymmetric buckling shapes, parallelly distributed load	27
2.5. Summary and principal results 1 and 2	31
3. Modelling the buckling edge as a compressed planar ring	33
3.1. Analytical model	33
3.2. Results	38
3.3. Summary and principal result 3	40
4. Analysis of buckling shapes with discrete symmetry of revolution	41
4.1. Description of buckling shapes with discrete symmetry of revolution	41
4.2. Analytical model	42
4.3. Results	49
4.4. Summary and principal results 4 (excluded result 4.3) and 5	56

5. Experiments and FE analyses	58
5.1. Experiments	58
5.2. FE analyses	61
5.3. Summary and principal result 4.3	62
6. Summary and principal results	63
Acknowledgements	69
Publications connected to the principal results	70
Other publications in the subject of the research topic	71
Publications connected to the research topic in respects of the history of architecture	72
Publications in the topic of structural engineering	73
References	74
APPENDICES	I
Appendix A	I
Appendix B	XII

Brief summary

The problem of spherical shell buckling is still current. Even now there exists a noticeable difference between theoretical and experimental results, which cannot be explained only by the imperfections, material nonlinearities and other effects that were not taken into account. Most differences can originate from the incompleteness of theoretical models.

The goal of my research is to determine the buckling shape of point-loaded spherical shells. Additionally, the load-deflection function is also to be determined. To achieve these results, an analytical model was developed, which shows us the possible buckling shapes for spherical shells, and also the load-deflection diagrams connected to them. The proposed model considers quasi-inextensional (quasi-isometric) buckling shapes with axisymmetry or discrete symmetry of revolution. An approximate model – based on engineering intuition – was also developed, which considers only the point where the axisymmetric buckling shape transforms into a shape that has discrete symmetry of revolution.

The proposed model gives us relatively precise solution for the load-deflection function of spherical shells. By means of the model the number of sides of buckling polygons can also be determined. Although this model is a qualitative one, it is worth mentioning that the obtained results are in good agreement with my experimental and numerical (FE) results. It can be stated based on the results of the model that the possible number of sides of buckling polygons increases monotonically with the radius-thickness ratio.

Polygonal buckling of spherical shells is a complex and still unsolved problem, which cannot be examined with usual tools. Despite the simplifications that were made in my models, the results enlighten many interesting phenomena and answer some of the most important questions. It is evident that further research is needed in this field.

Brief summary in Hungarian – Rövid összefoglalás

A gömbhéjak horpadásának vizsgálata jelenleg is aktuális kutatási téma. Az elméleti és kísérleti eredmények között jelentős eltérés tapasztalható, mely nem magyarázható kizárólag az imperfekciókkal, anyagi inhomogenitással és egyéb figyelembe nem vett hatásokkal. A különbségek jelentős részben az elméleti modellek tökéletlenségéből származnak.

Kutatásom célja, hogy a koncentrált erővel terhelt gömbhéj horpadási alakját meghatározzam. Emellett fontos cél a horpadáshoz tartozó teher-elmozdulás függvény meghatározása. Analitikus modellt dolgoztam ki, amelynek segítségével meghatározhatjuk a héj lehetséges horpadási alakjait és a horpadáshoz tartozó teher-elmozdulás diagramot. A modell kvázi-nyúlásmentes (kvázi-izometrikus) horpadási alakot feltételez, mely lehet körszimmetrikus vagy diszkrét forgásszimmetrikus. Mérnöki intuícióra alapozva egy közelítő modell is kidolgozásra került, mely kizárólag a körszimmetrikus horpadási alak diszkrét forgásszimmetrikus alakká történő átalakulását vizsgálja.

A modell segítségével viszonylag pontosan meghatározható a gömbhéj teher-elmozdulás összefüggése. A modellel a horpadáskor létrejövő sokszög oldalainak lehetséges számát is meghatározhatjuk. Fontos megjegyezni, hogy a modell kvalitatív jellege ellenére a kapott eredmények összhangban vannak az általam elvégzett kísérleti és numerikus (végesesemes) eredményekkel. A modell által szolgáltatott eredmények alapján megállapítható, hogy a horpadási sokszög oldalainak száma a sugár-vastagság arány monoton növekvő függvénye.

A gömbhéjak poligonális horpadása összetett és jelenleg nem megoldott feladat, mely nem vizsgálható hagyományos eszközökkel. A bemutatott modellekben tett egyszerűsítések ellenére az eredmények számos érdekes jelenséget megvilágítanak és több fontos kérdést is megválaszolnak. Megállapítható, hogy a terület további kutatást igényel.

1. Introduction

*Although nature commences with reason
and ends in experience it is necessary for us
to do the opposite, that is to commence
with experience and from this to proceed to
investigate the reason.*

(Leonardo da Vinci, 1452-1519)

1.1. Background of the research, motivation

Large deflection analysis of thin elastic shells plays an essential role in mechanics and other fields of science. Shells constitute a special group among surface structures. Surface structures are structures with small (generally negligible) thickness compared to their other dimensions. Shells are surface structures that have (once or twice) curved middle surfaces (*Csonka, 1981, Hegedűs, 1998*).

The dissertation investigates spherical shells. It is necessary to have a short overview on research topics that focus on the behaviour of characteristically elliptic surface structures. Domes (Figure 1.1.) and other shell structures (Figure 1.2.) require sufficient safety against buckling, and their performed deformations should also be limited, even in the case of special loads (e.g. dynamic wind loads). Structural elements of aircraft and aerospace vehicles (Figure 1.3.) should naturally also be dimensioned for sufficient safety against buckling (*Bushnell, 1985*). Containers (Figure 1.4.) and pressure vessels (*Dinno-Gill, 1974, Gould, 1988*) are subjected to internal pressure, which can also cause buckling, even if they are only partially filled (*Singer et al, 2002*). The characteristic (i.e. the load-deflection function) of micro switches in electronics or diaphragm clutch springs of motor vehicles in mechanical engineering is also an important issue. In nanoscience (*Falco et al, 2011*) (Figure 1.5.), the behaviour of nano-sized spheres adhering onto a rigid substrate is a current research topic (*Komura et al, 2005*). The buckling of shell-like colloid particles caused by a drying-induced internal

vacuum (*Tsapis et al, 2005*) (Figure 1.6.) is a substantial aspect in physical chemistry (*Quilliet et al, 2008*). The effect of physical circumstances in morphogenesis (*Forgács, 1996*) (Figure 1.7.) is a key issue in biology (*Moulton et al, 2012, Steele, 2000*). The behaviour of biomimetic polymer layers (*Feinberg et al, 2007*), or viruses and living cells (*Hutchinson et al, 2016*) (Figure 1.8.) can establish a close connection to thin shell theory, when their deformations are being investigated (*Vliegenthart-Gompper, 2011*). If the heart and the cardiovascular system (*Gould, 1988, Wong-Rautaharju, 1968*) are being modelled, a coupled model is needed to analyse the fluid-structure interaction. In medical sciences the packing of medicines should be mentioned as an important field of research (*Prausnitz-Langer, 2008*).

Buckling of spherical shells was a relevant research topic in the 20th century, as it is described in references (*El Naschie, 1990, Hegedűs, 1998, Kollár-Dulácska, 1984*). Nowadays the above mentioned problem is also in focus because of the increasing importance of thin structures and the improvement of numerical techniques. Generally, it is not easy to determine the connection between the load and the deflection of shells. Even now there exists a noticeable difference between theoretical and experimental results, which cannot be explained only by the imperfections, material nonlinearities and other effects that were not taken into account. Most differences can originate from the incompleteness of theoretical models.



Figure 1.1.: Dome of St. Peter's Basilica, Rome (photo by the author)



*Figure 1.2.: Reinforced concrete shell structure of Kelenföld bus garage, Budapest
(photo by the author)*



Figure 1.3.: Close-up of aircraft MiG-15, Szolnok (photo by the author)



Figure 1.4.: Spherical container at Csepel, Budapest (photo by the author)

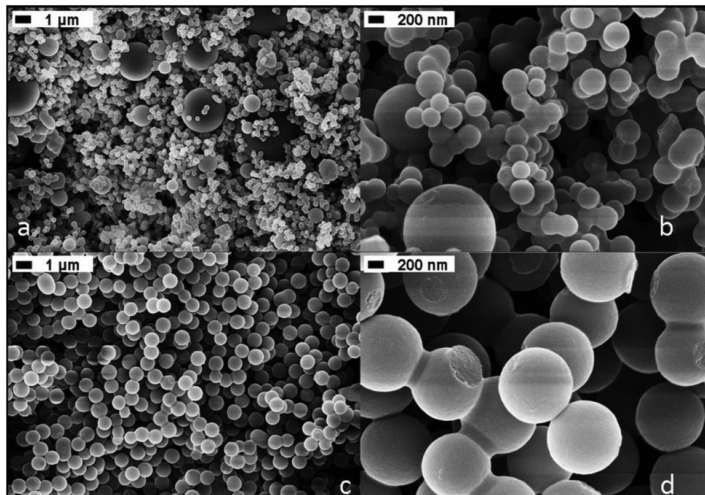


Figure 1.5.: Nano-sized spherical structures (photo by kind permission of M-M. Titirici (Falco et al, 2011))

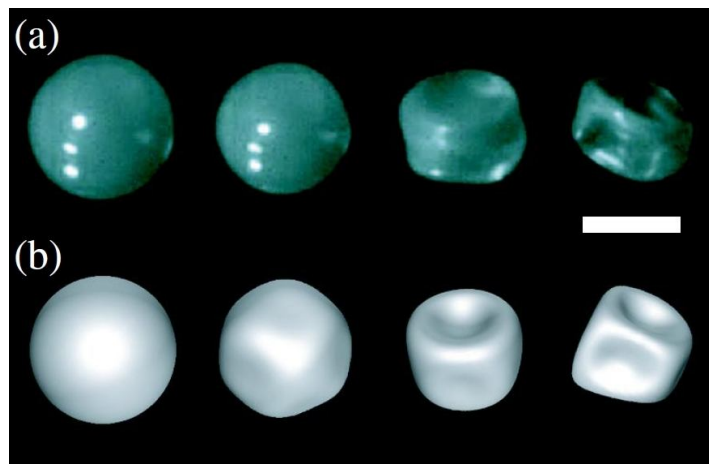


Figure 1.6.: Colloid particles (photo by kind permission of N. Tsapis (Tsapis et al, 2005))

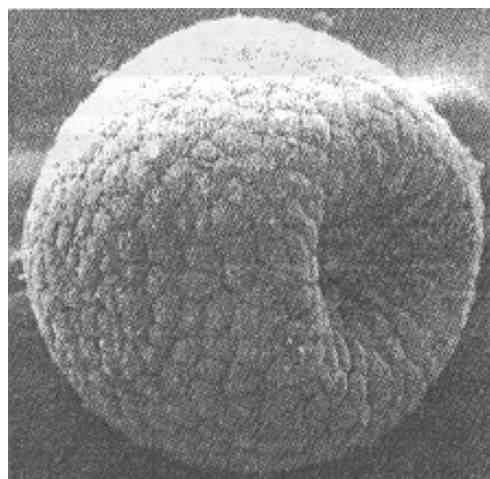


Figure 1.7.: Morphogenesis (photo by kind permission of G. Gorgács (Forgács, 1996))

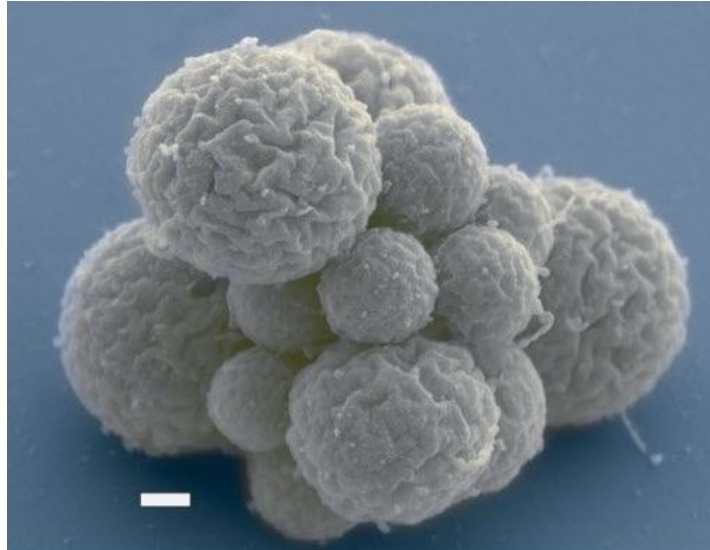


Figure 1.8.: Living spherical cells (photo by kind permission of C. A. Hutchinson (Hutchinson et al, 2016))

Researchers used to consider axisymmetric buckling shapes (Evkin, 2005, Kollár-Dulácska, 1984, Pogorelov, 1988, Thang, 1989, Wolmir, 1962, Zhu et al, 2002), although buckling shapes are usually non-axisymmetric (polygonal), as it can be seen in some recent works (Antman, 2005, Audoly-Pomeau, 2010, Galpin et al, 2008, Grolleau et al, 2008, Gupta et al, 2008, Knoche-Kierfeld, 2014, Pauchard-Rica, 1998, Vaziri-Mahadevan, 2008, Vaziri, 2009), or in everyday life (e.g. buckling of plastic packaging materials or ping-pong balls, Figure 1.9.). Sometimes the phenomenon of polygonal buckling induces a new idea in research, e.g. the Buckliball (Shim et al, 2012). It is stated by the researchers that the problem of the buckling of spherical shells has not been solved yet; therefore, the topic needs further investigation (Audoly-Pomeau, 2010, Vaziri, 2009).



Figure 1.9.: Buckling shapes of a ping-pong ball: circular shape at smaller deflection, polygonal shape at larger deflection (photo by the author)

There are several results available in literature for non-axisymmetric (polygonal) buckling of point-loaded spherical shells. Although the same situation is being examined, the statements are sometimes different. The non-axisymmetric shape is discussed (Pogorelov, 1963), and a critical load is determined for the transformation into polygonal shape. Bushnell and Penning (Bushnell, 1967, Penning, 1966) state that the number of sides of buckling polygons can only be three, four or five. The order of their appearance during loading is basically this, but – as it is stated – experiments sometimes show some differences. Fitch (Fitch, 1968) claims that the buckling polygon generally does not change during loading, the number of the sides of the buckling polygons depend on the relative thickness (radius-thickness ratio) of the shell. Thicker shells exhibit axisymmetric shapes or pentagons; at thinner shells one can see squares or triangles. Tarnai (Tarnai, 1989) examines a very thin shell with a mandrel inside the specimen, which is subjected to vacuum loading. This is not the same case as the cases considered by most of the researchers, but it is worth mentioning because of the complex, well-developed honeycomb pattern on the whole shell surface consisting of pentagons and hexagons. Pauchard and Rica (Pauchard-Rica, 1998) discuss the case of point-loaded spherical shells, and their statement is that the buckling shape changes as follows: circle, ellipse, triangle, square, pentagon. Galpin, Grolleau et al. (Galpin et al, 2008, Grolleau et al, 2008) claim that the reason for the appearance of polygons is the material anisotropy caused by the manufacturing process of the shell. Vaziri et al. (Vaziri-Mahadevan, 2008, Vaziri, 2009) state that the order of shapes is almost the same (excluding ellipse) as can be read in the article of Pauchard and Rica (Pauchard-Rica,

1998). They give a formula for the points of appearance of these shapes, depending on the relative thickness (radius-thickness ratio) of the shell. The case of flat rigid plate indentation is also considered, where the statement is that only pentagons appear at thicker shells, whereas only squares appear at thinner shells. Quilliet et al. (*Quilliet et al, 2008*) examine very small spherical shells (colloid particles) subjected to vacuum loading. The patterns on the buckled shell depend on the relative thickness. Knoche and Kierfeld (*Knoche-Kierfeld, 2014*) discuss three different types of buckling: the first buckling (lower critical load), the classical buckling (upper critical load) and the second buckling. Between the load levels of the first two types of buckling (the first and the classical buckling) the shell can either be in an unbuckled state or in a buckled state with axisymmetric pattern. Above the load level of the last type of buckling (the second buckling), the shell is certainly in a buckled state with non-axisymmetric pattern. In the light of these, it can be declared that the problem of spherical shell buckling is still current, with many substantial questions answered differently or not yet answered.

1.2. The goal of the research

The goal of my research is to determine the buckling shape of point-loaded spherical shells. Although shells are usually loaded with distributed loads, according to the book of Menyhárd (*Menyhárd, 1966*), sometimes loading with a concentrated force plays an important role, particularly in the case of the buckling of small shells. Additionally, the load-deflection function is also to be determined. To achieve these results, an analytical model was developed, which shows the possible buckling shapes for spherical shells, and also the load-deflection diagrams connected to them. According to the model, spherical shells first buckle in an axisymmetric shape, then this shape changes to a non-axisymmetric (polygonal) one if the load is increased. This phenomenon can usually be seen in experiments (Figure 1.9.). In the research, only regular polygons were taken into account among the possible non-axisymmetric shapes. These shapes have discrete symmetry of revolution. An approximate model – based on engineering intuition – was also developed, which only considers the point where the axisymmetric buckling shape transforms into a shape that has discrete symmetry of revolution. This shows which type of polygon is chosen by the shell at this point. Experimental and numerical (FE) results verify my models.

1.3. Basic assumptions

Complete spherical shells are analysed in the research – except for Chapter 5. The reason for the consideration of complete spheres is the exclusion of the effects of the supports of the shell. In Chapter 5, the experiments and FE analyses are performed on half-spheres because of simplicity. Geometric imperfections, as well as material inhomogeneities and anisotropies are disregarded. The reason for the exclusion of geometric imperfections is that shell models based on inextensional or quasi-inextensional deformations are insensitive for imperfections (*Croll, 1975*). Thin shells are considered (the thickness-radius ratio is small), the thickness of the shell is assumed to be constant (and remains unchanged after deformation), and shear deformations are neglected. The material is assumed to be perfectly linearly elastic, without any plastic behaviour at all. The load of the shell is concentrated load, except for Chapter 2, where the case of parallelly distributed load is also considered. The load is symmetric to a plane that is perpendicular to the load vector(s) and it contains the centre of the sphere. Thus, it guarantees that the shell remains in equilibrium without any support.

The deformed shape of the shell is assumed to have symmetry of revolution. This symmetry of revolution can be continuous or discrete (shapes with discrete symmetry of revolution are considered to have mirror-symmetry at the same time). Continuous symmetry of revolution belongs to the case of circular buckling shapes (Chapter 2). In contrast, discrete symmetry of revolution belongs to the case of polygonal buckling shapes (Chapters 3, 4, and 5), where it has to be emphasized that this means regular polygons.

2. Analysis of axisymmetric buckling shapes

2.1. Inextensional (isometric) deformations

There are many possibilities to approximate the surface of a buckled spherical shell. Geometric description of the deformed shell surface in a postcritical state was introduced by Yoshimura, Kirste and Pogorelov (*El Naschie, 1990*). The geometric method (developed in the 50s) of A. V. Pogorelov, the famous Ukrainian mathematician was used in research because it is the most informative and complete (*Pogorelov, 1988*). The buckling shape in this model is achieved by isometric transformation of the original shell surface. The buckling load is considered using this basic assumption. For the introduction of the concept of isometric transformations it is important to describe some essential phenomena of surfaces.

Generally, deformations of surfaces are composed of stretching and bending. Considering a deformed surface, stretching means the (positive or negative) change in arc lengths measured on the surface. In other words, stretching means the change of metric – the metric is formulated by the first fundamental form of surfaces, see e.g. reference (*Bronstein et al, 2002*). Deformations that keep metric unchanged are called isometric transformations or inextensional deformations. Bending means the (positive or negative) change in curvatures of the surface. Bending can take place in the case of inextensional deformations, in a way that the metric of the surface does not change (*Hegedűs, 1998*).

Theoretically, both types of deformations (stretching and bending) can occur simultaneously in a shell structure, but in practice, usually only bending deformations take place on almost the entire shell surface. The reason can be found in the mechanics of thin elastic structures. Stretching rigidity (K_s) and bending rigidity (K_b) depend differently on shell thickness (*Flügge, 1973*):

$$K_s = \frac{Et}{1-\nu^2}, \quad (2.1)$$

$$K_b = \frac{Et^3}{12(1-\nu^2)}. \quad (2.2)$$

In equation (2.1) and (2.2) E is Young's modulus, t is the thickness of the shell, ν is Poisson's ratio. It can easily be recognised that if $t \rightarrow 0$ then $K_b / K_s \rightarrow 0$, so if the thickness of the shell decreases, stretching rigidity suppresses bending rigidity. This results in the fact that no significant stretching deformations take place in a thin shell, because it would require too much energy (*Ramm-Wall, 2004*). This leads to the idea of inextensional deformations of thin surfaces, especially thin shells. Inextensional deformations play a key role in the analysis of thin structures (*Croll, 1975, Ivanova-Pastrone, 2002*).

Many significant and interesting statements can be read about inextensional deformations in literature. Probably the most important fact is that infinitesimally thin surfaces can be divided into two groups: geometrically rigid and non-rigid surfaces (*Audoly, 2000*). A surface is called geometrically rigid if no sets of continuous isometric deformations exist in a small neighbourhood of the initial geometry of the surface. A closed complete sphere is a typical example for geometrically rigid surfaces. The only possible isometric deformation for a sphere is made by means of intersection of the sphere and a plane. The cut-off part of the sphere has to be mirror-reflected to the plane. The new shape is an isometric transformed form of the sphere, but it cannot be achieved continuously from the original shape by isometric transformation. The transformation can only be made through the stretching deformations of a certain part of a surface. It is evident that surfaces that do not belong to the group of geometrically rigid surfaces are geometrically non-rigid ones. A planar sheet is a typical example for geometrically non-rigid surfaces. It can be subjected to a variety of continuous isometric deformations.

Surfaces in reality have finite thickness, so they are not infinitesimally thin. In the case of thin surface structures, typically locally inextensional or quasi-inextensional deformations occur (*Vetř-Sajtos, 2016a, Vetř-Sajtos, 2016b*). In reality, only the geometrically non-rigid surfaces (e.g. the planar sheet) can show inextensional (isometric) deformations. Geometrically rigid surfaces (e.g. the closed complete sphere) often show locally inextensional (locally isometric) or quasi-inextensional (quasi-isometric) deformations. This means that almost the entire surface remains in inextensional state, except for relatively small zones where relatively large stretching deformations can be observed (*Ivanova-Pastrone, 2002, Pogorelov, 1988*). In the case

of a spherical surface, a series of these deformations can be observed typically. At small values of deflection, a certain part of the surface becomes flat (it does not sustain mirror-reflection), then, if deflection is increased, a shape close to the mirror-reflected isometric transformed shape of the sphere appears. By further increase of deflection, a more complex pattern evolves on the surface, as it is shown in Figure 2.1. These shapes have a common feature: there are large parts where strain energy belonging to bending deformations is significant while strain energy belonging to stretching deformations is relatively small (*Croll, 1975, El Naschie, 1990*). Stretching deformation energy is localised into ridges. These states can be called locally inextensional (locally isometric) or quasi-inextensional (quasi-isometric). The idea of quasi-inextensional deformations of cylindrical and hyperboloid shells also appear in (*Croll, 1975*).

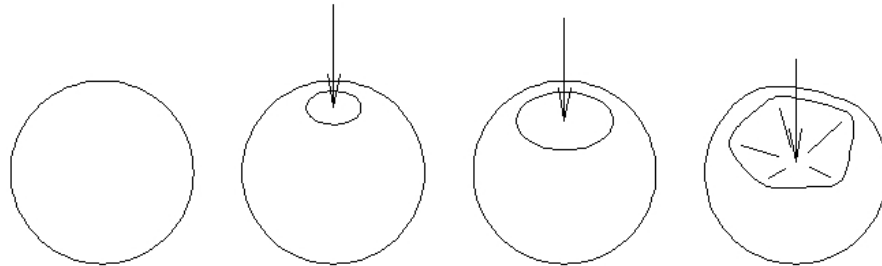


Figure 2.1.: Possible quasi-isometric (quasi-inextensional) deformations of a geometrically rigid surface (e.g. a ping-pong ball)

The same approach is discussed in detail in reference (*Ivanova-Pastrone, 2002*) for the analysis of the geometry of deformed shell surfaces. The main point of this concept is that generally the possible isometric transformed shapes of geometrically rigid shells (obtained by bending deformations) are irregular (i.e. edges appear on the deformed surface between its regular parts). Nevertheless, deformed shapes of shells with finite thickness should be regular, so in the edges an isometry-breaking set of stretching deformations occurs, which does not considerably change the overall geometry of the deformed surface. In other words, stretching deformations in edges are needed to match the isometric transformed pieces of the deformed shell surface. The result is a locally inextensional (locally isometric) or quasi-inextensional (quasi-isometric) surface, in agreement with references (*Croll, 1975, El Naschie, 1990*). In the dissertation, these deformations of shells in the applied models are called quasi-inextensional (quasi-isometric).

On the basis of these considerations, it can be stated that shells can have various quasi-inextensional states. Experiments (*Vető-Sajtos, 2014, Vető-Sajtos, 2016a*) show that buckling shapes with discrete symmetry of revolution evolve from axisymmetric buckling shapes. The question arises whether there is a possibility for a continuous inextensional transformation between these shapes (i.e. circular and polygonal shapes). If infinitesimally thin shells are considered, the question can be formulated as follows: is there a possibility for two spherical caps (prepared from a complete spherical shell by intersection with a plane, joined as it is shown by Figure 2.2.) to exhibit continuous inextensional deformations forbidding any relative displacements at their common edges? The solution can be found relatively easily using the expressions of inextensional deformations of spherical caps.

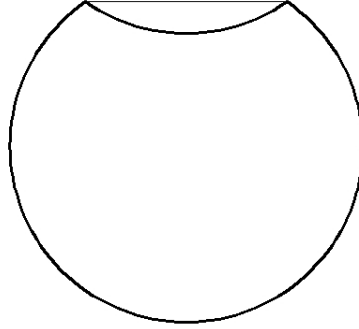


Figure 2.2.: Section of two spherical caps (prepared from a complete spherical shell by intersection with a plane) with edges joined (forbidding relative displacements)

Inextensional deformations of a spherical cap cause the following displacements at the edges (*Niordson, 1985*):

$$w^* = \left(A_m (m + \cos \theta) \tan^m \frac{1}{2} \theta \right) \cos m \phi, \quad (2.3)$$

$$u^* = \left(-A_m \tan^m \frac{1}{2} \theta \right) \sin \theta \cos m \phi, \quad (2.4)$$

$$v^* = \left(-A_m \tan^m \frac{1}{2} \theta \right) \sin \theta \sin m \phi, \quad (2.5)$$

where w^* is the normal, u^* and v^* are the tangential components of edge displacements, A_m is an arbitrary constant (which can be regarded as a scaling factor of the amplitude of displacements), θ is the meridional angle, ϕ is the circumferential angle, m is a positive integer, greater than 1, which denotes the wave number of displacements in the circumferential direction. If the relative displacements between the edges of the two spherical caps are set to be zero (i.e. edges have the same displacements), the following equations, which are not contained in reference (Niordson, 1985), are valid:

$$A_{m,1}(m + \cos \theta_1) \tan^m \frac{1}{2} \theta_1 = A_{m,2}(m + \cos \theta_2) \tan^m \frac{1}{2} \theta_2, \quad (2.6)$$

$$-A_{m,1} \tan^m \frac{1}{2} \theta_1 \sin \theta_1 = -A_{m,2} \tan^m \frac{1}{2} \theta_2 \sin \theta_2, \quad (2.7)$$

where $A_{m,1}$, θ_1 , $A_{m,2}$, and θ_2 belong to the two spherical caps, respectively. Displacements u^* and v^* in formulae (2.4) and (2.5) differ only by a factor depending on ϕ . This leads to the fact that equation (2.7) is enough to make the relative displacements between the edges zero in these directions. Equations (2.6) and (2.7) can be expressed in the form of a system of linear equations for $A_{m,1}$ and $A_{m,2}$:

$$\begin{bmatrix} (m + \cos \theta_1) \tan^m \frac{1}{2} \theta_1 & -(m + \cos \theta_2) \tan^m \frac{1}{2} \theta_2 \\ -\tan^m \frac{1}{2} \theta_1 \sin \theta_1 & \tan^m \frac{1}{2} \theta_2 \sin \theta_2 \end{bmatrix} \begin{bmatrix} A_{m,1} \\ A_{m,2} \end{bmatrix} = \begin{bmatrix} 0 \\ 0 \end{bmatrix}. \quad (2.8)$$

The two spherical caps in this problem are prepared from the same sphere, so θ_1 and θ_2 can be expressed with each other ($\theta_1 + \theta_2 = \pi$). Then equation (2.8) can be written as follows:

$$\begin{bmatrix} (m + \cos \theta_1) \tan^m \frac{1}{2} \theta_1 & -(m + \cos \theta_1) \cot^m \frac{1}{2} \theta_1 \\ -\tan^m \frac{1}{2} \theta_1 \sin \theta_1 & \cot^m \frac{1}{2} \theta_1 \sin \theta_1 \end{bmatrix} \begin{bmatrix} A_{m,1} \\ A_{m,2} \end{bmatrix} = \begin{bmatrix} 0 \\ 0 \end{bmatrix}. \quad (2.9)$$

This system of equations has nontrivial solutions if the determinant of the coefficient matrix is equal to zero. This implies a solution which is independent of m , the wave number of displacements in the circumferential direction:

$$\theta_1 = \frac{k\pi}{2}, \quad (2.10)$$

where k is a positive integer. This means that two spherical caps (prepared from a complete spherical shell) can exhibit continuous inextensional deformations only if the meridional angle is $\pi/2$, if any relative displacements at their common edges are forbidden (i.e. the edges have the same displacements). This is the case of two coinciding spherical half-caps, which can be disregarded in an engineering point of view. Therefore, generally the possibility of continuous inextensional deformations of spherical caps (joined in the above described way) does not exist (*Vető-Sajtos, 2016b*). This case has not been examined previously by engineers according to the literature, although the result is supported by engineering intuition.

On the basis of these results, it can be stated that there is no possibility for continuous inextensional deformations between buckling shapes with axisymmetry and discrete symmetry of revolution. Hence, only a considerable change of the load level can result in the change of the configuration of the buckling shape, because stretching deformations should occur. It means that there is necessarily a difference between the load-deflection functions of the buckling shapes with axisymmetry and discrete symmetry of revolution.

2.2. Energy method

Generally a strong distinction is made between small and large deflections in mechanics. If the buckling of shells is examined, a large deflection analysis is needed. The reason is that in this case significant (i.e. much larger than the thickness) displacements take place on a considerably large part of the surface. There is a strong distinction between small and large deformations (strains), as well.

Mechanical models based on small deformations are always simpler than the ones based on large deformations. In these models, the displacements of the structure (beam, plate, shell or a solid) do not cause considerable deformations in all possible

directions. For example, if a straight beam sustains displacements perpendicularly to its axis, only bending (and sometimes shear) deformations are taken into account. The axial deformations remain negligible. This method can be used only if displacements are small enough in relation to the dimensions of the structure. Small deformation models can also be thought of as simplified versions of the general models: large deformation models can be used for all mechanical problems (theoretically they give exact solutions). If a small deformation model is used instead of a large deformation one, the solution of a certain problem can be simplified substantially. Simplifications are based on observations and engineering intuition in a way that inevitable errors of the solution remain acceptable. For example, in the case of buckling of shell structures there are large deformations on some parts of the surface, but on other parts the deformations are negligible. It is not always easy to decide how to solve a certain problem, but it is sure that application of large deformation model for the whole surface would not be economical. In the cases discussed in the dissertation, small deformation (linearised) models are used, keeping in mind that deflections are large.

Buckling of spherical shells can cause large deflections and large deformations on certain parts of the surface. If displacements and strains (which are calculated by derivation of the displacements) are not directly used in a shell problem, categorization by magnitude of deflections and deformations becomes unnecessary. This way of solution is possible by the energy method.

Energy method is based on the principle of stationary potential energy, which is applied here for shell structures. Generally, the total potential energy is a functional, but in the dissertation the total potential energy W depends only on scalar variables (i.e. it is a function). In the present chapter the total potential energy is expressed with only one scalar displacement variable, which refers to the deflection of the shell (*Pogorelov, 1988*). In Chapter 4, where energy method is also used, three scalar displacement variables determine the total potential energy. Generally, the structure is in equilibrium if the partial derivatives of W vanish:

$$\frac{\partial W}{\partial x_i} = 0, \quad i = 1, 2, \dots, n, \quad (2.11)$$

where W is the function of total potential energy, $x_i, i=1, 2, \dots, n$ is the set of possible displacement variables, n is the number of displacement variables (in the present

chapter, $n = 1$, while in Chapter 4, $n = 3$). The equilibrium state obtained by satisfying (2.11) is stable if the Hessian matrix (composed of the second partial derivatives) is positive definite. In the problem of the present chapter (where W has only one displacement variable) this matrix has only one element, so it is easy to calculate. In the problem of Chapter 4 (where W has three displacement variables) the equilibrium states and their stability are analysed by numerical methods, converting the problem to the (numerical) minimum seeking of the function of total potential energy W .

The total potential energy can be composed of the strain energy of the deformed structure and the work performed by the loads along the displacements. The expression – using Pogorelov’s notations (*Pogorelov, 1988*) – is as follows:

$$W = U - A, \tag{2.12}$$

where U is the strain energy, A is the work performed by the loads. To determine these values, calculation of some displacements and strains is obviously needed, but it is enough to calculate them only for the supposed equilibrium state. The complete “path” leading to this state is not relevant here. If the deformed shape can be described with more than one variable, the energy method remains easy to handle.

As a justification of using the above described method to find the equilibrium states of spherical shells in the post-buckling range, a general load-deflection diagram of shells with unstable initial post-buckling state should be discussed (*El Naschie, 1990*), see Figure 2.3. The equilibrium path of the perfect shell bifurcates at the linear critical load level, and the buckling starts with an unstable load-deflection curve. The diagram has a minimum point (which belongs to the lower critical load), where it regains its stability. The behaviour of the imperfect shell is different: no bifurcation can be seen, the diagram has a maximum point (which belongs to the upper critical load). The value of the upper critical load is highly determined by initial geometric imperfections (*Kollár-Dulácska, 1984*), and reaches only a fragment of the value of the linear critical load. Because of its high imperfection-sensitivity, the upper critical load is not applicable for structural design. The diagram of the imperfect shell also has a minimum point, which is not really influenced by imperfections (i.e. the imperfect shell almost reaches the lower critical load of the perfect shell). The imperfection-insensitivity of the lower critical load makes it applicable for structural design. This imperfection-insensitivity is also formulated by Croll (*Croll, 1975*), and it makes us

possible to neglect initial geometric imperfections in calculations presented in the dissertation.

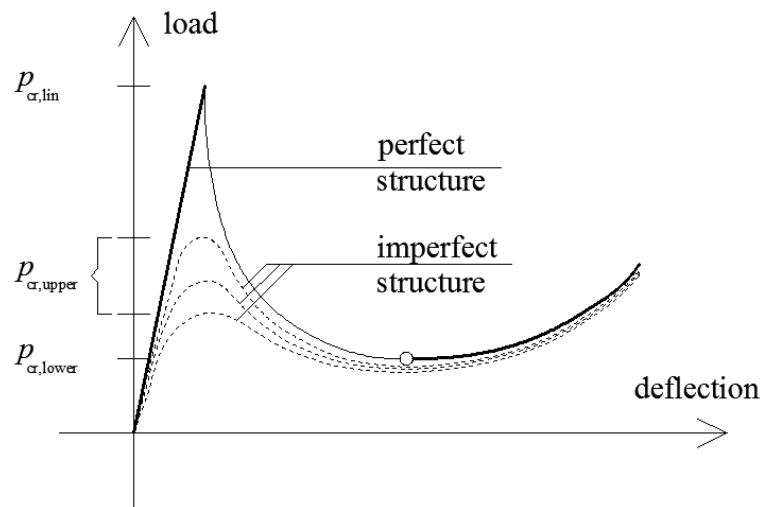


Figure 2.3.: General load-deflection diagram of shells with unstable initial post-buckling state

2.3. Axisymmetric buckling shapes, concentrated force – Pogorelov’s results

The buckling shape of spherical shells is supposed to be axisymmetric in many publications (Evkin, 2005, Kollár-Dulácska, 1984, Pogorelov, 1988, Thang, 1989, Zhu et al, 2002). This axisymmetric buckling shape can be regarded as the quasi-isometric transformed shape of the original spherical surface, because there are no deformations outside the buckling edge, and there are only bending deformations inside the circle of the buckling edge. Stretching deformations occur only in the small neighbourhood of the buckling edge, which is a relatively small part of the surface.

Pogorelov gives an elaborate description of the geometric method used for his research on the buckling of spherical shells. Here only the most important parts are presented from his widely referred book (Pogorelov, 1988), which are inevitably needed in order to understand his method and to discuss the results. As a remark, the method of Pogorelov is also presented in the dissertation of Knoche (Knoche, 2014), which indicates the recent interest in the topic.

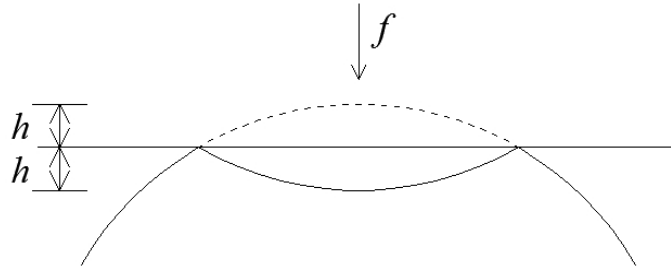


Figure 2.4.: Section of a spherical shell, considering axisymmetric buckling shape and concentrated force

Pogorelov neglects the effect of supports. He supposes an axisymmetric buckling shape, which is the quasi-isometric transformed shape of the original surface. The axis of symmetry is the line of action of the concentrated force f . The shape is obtained by means of intersection of the sphere and a plane which is perpendicular to the line of action of the load. The cut-off part of the sphere is mirror-reflected to the plane (Figure 2.4.). Naturally f is a conservative force, because its work done in moving a structure or a structural part between two points is independent of the taken path. The work performed by the load is relatively easy to calculate:

$$A = 2fh, \quad (2.13)$$

where f is the concentrated force, h is the half of the total central deflection, see Figure 2.4.

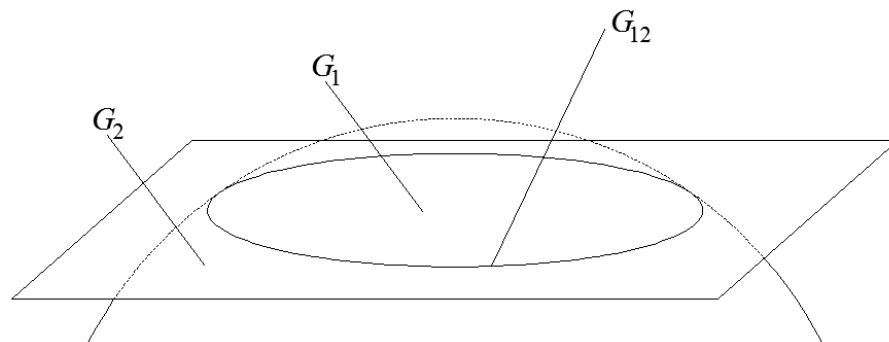


Figure 2.5.: Division of axisymmetrically buckled spherical shell surface into parts, in order to determine the strain energy: G_1 is mirror-reflected (bending deformations), G_2 is undeformed (no deformations), G_{12} joins G_1 and G_2 (stretching and bending deformations)

Calculation of strain energy is a much more complicated task. According to the geometric features of the buckled surface, Pogorelov divides it into three parts: G_1 , G_2 , and G_{12} (Figure 2.5.). G_{12} is the narrow zone of the buckling edge, G_1 is the (buckled) part inside G_{12} , and G_2 is the (unbuckled) part outside G_{12} . On part G_2 no strain energy arises, so the total strain energy of the structure is:

$$U = U(G_1) + U(G_{12}). \quad (2.14)$$

Part G_1 has (mirror-reflected) spherical geometry, so the change of curvatures is $-2/R$ in all directions. It is assumed that there is no stretching energy on this surface part, so the strain energy is purely bending energy:

$$U(G_1) = \frac{Et^3}{3(1-\nu)} \frac{1}{R^2} S(G_1), \quad (2.15)$$

where E is Young's modulus, t is the thickness of the shell, ν is Poisson's ratio, R is the radius of the shell, $S(G_1)$ is the area of surface part G_1 . For the calculation of the strain energy on G_{12} , this part should be divided further into two: inner and outer part. The width of the buckling edge (zone G_{12}) is nonzero, and the inner part of G_{12} osculates to G_1 , the outer part osculates to G_2 (Figure 2.6.).

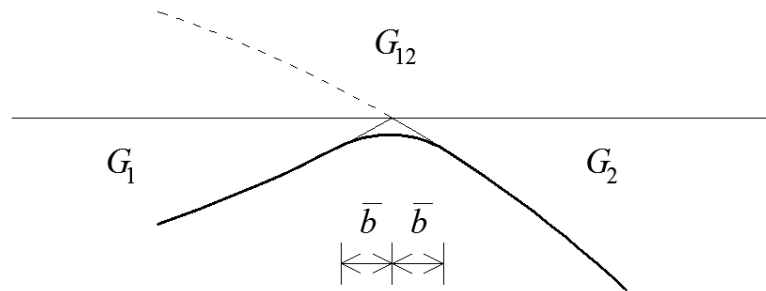


Figure 2.6.: Section of buckling edge (zone G_{12}), the difference between the isometric transformed shape (normal line) and the quasi-isometric transformed shape (bold line) can be examined

The stretching energy on G_{12} is the same in the inner and outer part, and it arises only in the circumferential direction. The bending energy on G_{12} can be calculated from the difference between the (theoretical) isometric transformed shape and the (practical)

quasi-isometric transformed shape. It can be formulated as follows, on the basis of the strains in the circumferential direction and the changes of curvatures in the meridional and the circumferential directions:

$$U(G_{12})_{inner} = 2\pi r K_b \int_0^{\bar{b}} \bar{v}'^2 ds + 2\pi r K_s^* \int_0^{\bar{b}} \frac{\bar{u}^{-2}}{r^2} ds - \frac{4(1+\nu)\pi r K_b \alpha}{R} + \pi r K_b \nu \frac{\alpha}{R}, \quad (2.16)$$

$$U(G_{12})_{outer} = 2\pi r K_b \int_0^{\bar{b}} \bar{v}'^2 ds + 2\pi r K_s^* \int_0^{\bar{b}} \frac{\bar{u}^{-2}}{r^2} ds - \pi r K_b \nu \frac{\alpha}{R}, \quad (2.17)$$

where r is the radius of the circular buckling edge, \bar{u} and \bar{v} denote the differences between the isometric transformed shape and the quasi-isometric transformed shape perpendicular and parallel to f , respectively, s is the arc length parameter in the meridional direction, \bar{b} is the half-width of G_{12} , α is the azimuth angle belonging to the buckling edge. K_b is the bending rigidity of the shell (2.1), K_s^* is a factor used by Pogorelov (*Pogorelov, 1988*), which is similar to stretching rigidity (2.2):

$$K_s^* = \frac{Et}{2}. \quad (2.18)$$

The real buckling shape of the shell – which is the quasi-isometric transformed shape of the original surface – is approximated well by the isometric transformed shape. Difference emerges only on G_{12} , but it does not affect the work performed by the load. Thus the actual buckling shape can be determined based on the minimum of the strain energy on G_{12} . The expressions for the inner and outer part (2.16 and 2.17) differ only by terms that do not depend on \bar{u} and \bar{v} , so they are the same in the process of minimization. So the subject of minimization is the following expression:

$$U(G_{12})_{inner} \sim U(G_{12})_{outer} \sim \pi r K_b \int_0^{\bar{b}} \bar{v}'^2 ds + \pi r K_s^* \int_0^{\bar{b}} \frac{\bar{u}^{-2}}{r^2} ds. \quad (2.19)$$

Certainly, there are boundary conditions for \bar{u} and \bar{v} . These conditions account for the osculation of G_1 , G_{12} , and G_2 . The boundary conditions are the following for the outer part of G_{12} :

$$\bar{v}'(0) = -\alpha, \quad \bar{v}'(\bar{b}) = 0, \quad \bar{u}(0) = 0, \quad \bar{u}(\bar{b}) = 0. \quad (2.20)$$

On the basis of these considerations, an interesting and ingenious solution method can be found for the minimization problem in the book of Pogorelov (*Pogorelov, 1988*). As a result, a closed formula is obtained for the strain energy of the total buckled surface:

$$U = \frac{2\pi c E t^{5/2} (2h)^{3/2}}{R}, \quad (2.21)$$

where $c = 0.19$ is a dimensionless constant gained during the minimization.

Approximations based on observations and engineering intuition were made to obtain the above result. Pogorelov states that the error of these approximations decreases as the thickness of the shell decreases (*Pogorelov, 1988*). The total potential energy is as follows:

$$W = U - A = \frac{2\pi c E t^{5/2} 2\sqrt{2} h^{3/2}}{R} - 2fh. \quad (2.22)$$

The formula for the equilibrium states is obtained by taking the first derivative of the above one:

$$f = 3\pi c E t^{5/2} \frac{\sqrt{2h}}{R}. \quad (2.23)$$

If the second derivative of W is also calculated (which is not presented here), it can be stated that expression (2.23) corresponds to stable equilibrium states. The concentrated force f increases monotonically with h , the central half-deflection of the buckled surface increases. The load-deflection diagram for this expression is shown in Figure 2.7. It can be stated that the load-deflection function does not give a minimum value (a lower

critical load) in the case of concentrated force, if axisymmetric buckling shapes are considered. The above described method and results are contained in (Pogorelov, 1988).

There is no bifurcation at positive values of h (Vető-Sajtos, 2009a). The “path” of equilibrium states belonging to the buckled shape gets off the “path” of the unbuckled (trivial) shape at zero load (and zero deflection). As a result of this analysis for concentrated load it can be stated that the shell gets into a buckled state at the very beginning of the loading process, according to this model. As a mechanical explanation, it is more favourable for the shell to buckle at a relatively small zone, because this requires relatively small stretching energy. If the load f is increased, only the size of the buckled region increases, however, no qualitative change happens to the shell, and no significant change occurs in the stretching energy.

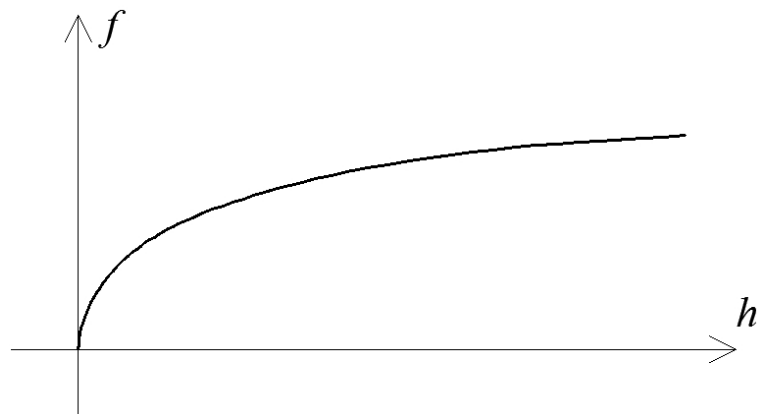


Figure 2.7.: Load-deflection diagram for axisymmetric buckling shape and concentrated force, the diagram shows only the curve belonging to the buckled state

2.4. Axisymmetric buckling shapes, parallelly distributed load

The case of a convex elliptic shell loaded with parallelly distributed load is discussed in the book of Pogorelov (Pogorelov, 1988). Here the (more special) case of spherical shell is considered (Figure 2.8.), according to (Vető-Sajtos, 2009a). The uniformly distributed load is conservative, similarly to the concentrated force in the previous section. Hence, the energy method is applicable.

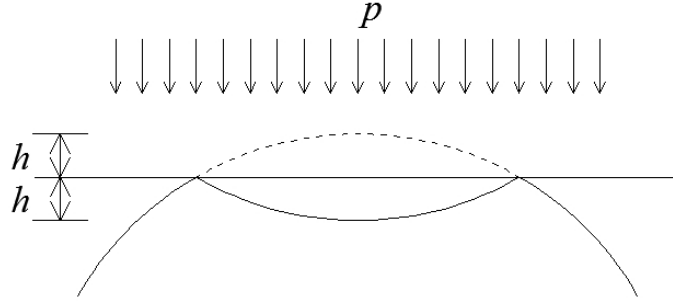


Figure 2.8.: Section of a spherical shell, considering axisymmetric buckling shape and parallelly distributed load

The buckling shape is assumed to be the same as in the case of the concentrated force, so expression (2.21) developed for strain energy can be used in the case of parallelly distributed load, as well. For the calculation of the work performed by the load, the volume between the unbuckled and the buckled surface has to be determined. According to my research (Vető-Sajtos, 2009a), the work of the load was determined as follows:

$$A = 2p\pi \left(h^2 R - \frac{h^3}{3} \right), \quad (2.24)$$

where p is the intensity of the load. For achieving expression (2.24), the formula for the volume of a spherical cap has been used, without any approximation. The total potential energy is determined by the following expression:

$$W = U - A = \frac{2\pi cEt^{5/2} 2\sqrt{2}h^{3/2}}{R} - 2p\pi \left(h^2 R - \frac{h^3}{3} \right), \quad (2.25)$$

and the load-deflection function based on the first derivative of W is as follows:

$$p = 3cEt^{5/2} \frac{\sqrt{2}h}{Rh(2R-h)}. \quad (2.26)$$

The load-deflection diagram of the case of parallelly distributed load can be seen in Figure 2.9. The load-deflection function has a minimum at $h = 2/3 R$. If the second derivative of function W is calculated, it can be stated that the load-deflection function

represents unstable equilibrium states for $h < 2/3 R$, and stable equilibrium states for $h > 2/3 R$. The load value at $h = 2/3 R$ belongs to the lower critical load of the shell (2.27). In the neighbourhood of $h = 2/3 R$ the load-deflection diagram is almost horizontal on a relatively large domain of h . Although this load value corresponds to a relatively large deflection, it is a lower bound for the postcritical load-bearing capacity (Vető-Sajtos, 2009a):

$$p_{cr,lower} = \frac{9\sqrt{3}}{4} cE \left(\frac{t}{R} \right)^{5/2}. \quad (2.27)$$

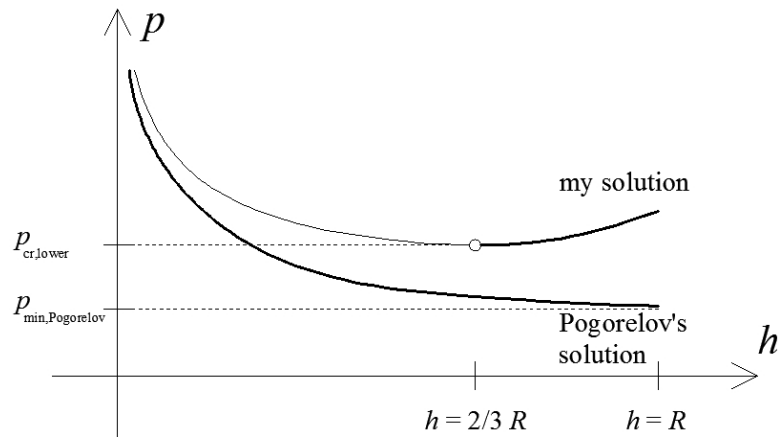


Figure 2.9.: Load-deflection diagram for axisymmetric buckling shape and parallelly distributed load, the diagram shows only the curves belonging to the buckled states

The book of Pogorelov (Pogorelov, 1988) discusses the general case of convex elliptic surfaces. This is the reason why the so-called osculating paraboloid is used for the calculation of the work performed by the load in his book. This contradicts my assumption that the buckled part of the spherical shell is an inverted spherical surface. At lower deflections this does not result in large error, but the difference cannot be neglected in the case of higher deflections. The load-deflection function obtained by Pogorelov:

$$p_{Pogorelov} = 3cE \frac{t^{5/2}}{R^2 \sqrt{2h}}. \quad (2.28)$$

This function does not have a minimum for h . Hence, there is no lower critical load, only the load level belonging to the largest possible deflection can be calculated:

$$p_{\min, \text{Pogorelov}} = \frac{3}{\sqrt{2}} cE \left(\frac{t}{R} \right)^{5/2}, \quad (2.29)$$

which is not more than the half of the load level determined by me at (2.27). Moreover, this belongs to such a large deflection which is unreal. Figure 2.9. shows Pogorelov's result for the general case of convex elliptic shells, as well.

It should be emphasized that the reason for the difference between the load-deflection functions determined by me and Pogorelov – described by expressions (2.26) and (2.28) – has a purely geometric origin. The difference is not the result of an incomplete series expansion: the volume of a spherical cap is used for the calculation of the work performed by the load in (2.24), while the volume of a paraboloid is used by Pogorelov (*Pogorelov, 1988*).

It is worth comparing the value of the lower critical load (2.27) with critical load values in references (*Kollár-Dulácska, 1984, Dulácska, 1987*), see Figure 2.10. The original publications of the authors appearing in Figure 2.10., namely Kármán-Tsien, Thompson, Dostanova-Raizer, and Csonka, are not referred here; their results are contained in references (*Kollár-Dulácska, 1984, Dulácska, 1987*). The difference between the critical load values is moderate. The value determined by Csonka is a sort of a universal lower bound. It was determined on the basis of the observations of a collapsed reinforced concrete shell structure in Gödöllő, Hungary (*Dulácska, 1987*).

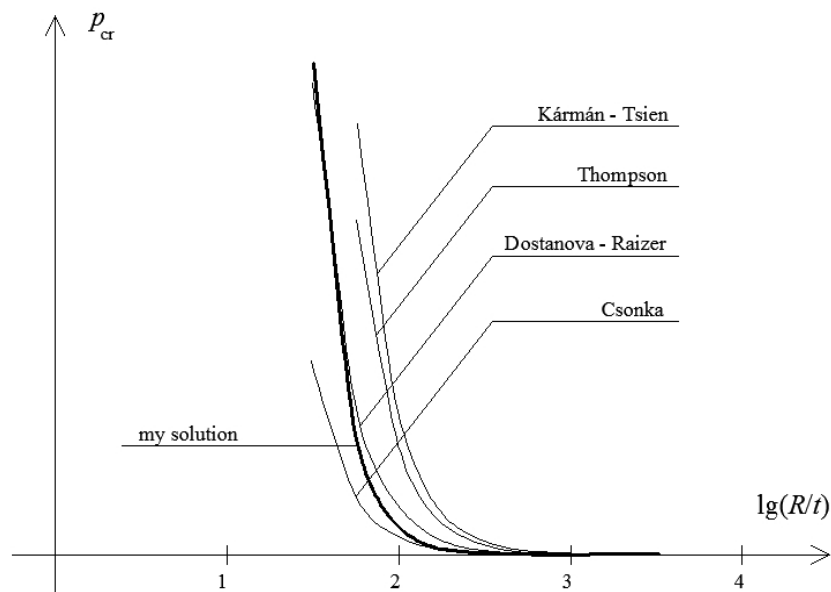


Figure 2.10.: Critical load of spherical shells – comparison, results are taken from references (*Kollár-Dulácska, 1984, Dulácska, 1987*)

2.5. Summary and principal results 1 and 2

If large deflections (e.g. buckling) of thin shells are considered, bending energy dominates stretching energy on most of the surface. Stretching energy is localised in edges and vertices. This leads to the idea of locally inextensional (locally isometric) or quasi-inextensional (quasi-isometric) deformations of thin surfaces (*Croll, 1975, El Naschie, 1990, Ivanova-Pastrone, 2002, Pogorelov, 1988*). The buckling shape of spherical shells can be approximated by isometric transformations of the original surface, assuming the buckled part to be an inverted spherical surface. In reality, the buckling shape is the quasi-isometric transformed shape of the original surface. Based on this consideration, the load-deflection function can be determined by means of Pogorelov's method (*Pogorelov, 1988, Knoche, 2014*). The energy method is used to determine the load-deflection function in different cases. In the case of concentrated force, Pogorelov's results are valid, while in the case of parallelly distributed load, new results are obtained. Additionally, it has been proved that the axisymmetric buckling shape of spherical shells generally cannot be transformed inextensionally into a buckling shape with discrete symmetry of revolution.

Principal result 1

(relevant publication: (*Vetř-Sajtos, 2009a*))

For spherical shells subjected to parallelly distributed load (which is distributed uniformly along the horizontal projection of the surface), considering the buckling shape as an axisymmetric quasi-isometric transformed shape of the shell, I determined analytically the load-deflection function in the post-buckling state and the lower critical load. The value of the lower critical load is in good agreement with analytical results obtained by different methods available in literature.

Principal result 2

(relevant publication: (*Vetř-Sajtos, 2016b*))

I proved that two spherical shell caps (which can realise inextensional deformations), derived from the same sphere by intersection with a plane, are not

able to perform inextensional deformations if their edges are joined in a way that the caps are located at the same side of the plane of the edges, except for the case of two half-spheres. Consequently, the axisymmetric buckling shape of spherical shells cannot be transformed inextensionally into a buckling shape with discrete symmetry of revolution, if the buckled part is smaller than the half of the sphere.

3. Modelling the buckling edge as a compressed planar ring

3.1. Analytical model

There is a plausible analogy between the circular buckling edge of the spherical shell and a planar elastic ring subjected to inward-pointing distributed load. The load results in compressive forces in the ring, while the other parts of the shell can serve as bedding. My research on the buckling shape of spherical shells can be supported by this analogous case, which is already discussed in literature, separated from shell theory. The buckling edge is not able to perform inextensional deformations in this configuration, see Section 2.1.

The formula for the critical load of a compressed elastic ring (3.8) is available in references (*Kollár, 1999*). Experiments show that the axisymmetric buckling edge of spherical shells transforms into a polygonal edge with discrete symmetry of revolution if the loads are increased. This is the basis of the assumption that the transformation of the originally circular buckling edge into a regular polygon can be regarded as the buckling of a planar elastic ring subjected to inward-pointing distributed load (*Vető-Sajtos, 2014, Vető-Sajtos, 2016a*).

The relationship between the two different structures is based on their structural behaviour. The compression force in the ring can be explained and determined by the membrane theory of shells. The load of the shell is only balanced by membrane forces in the total shell surface (except for the small neighbourhood of the concentrated force), thus generally vertical and horizontal internal force components of the meridional force exist simultaneously (Figure 3.1.). The inner and outer vertical components ($n_{\phi,z}$) at the buckling edge balance each other, while the inner and outer horizontal components ($n_{\phi,\rho}$) are added to each other and thus they load the ring in its plane with an inward-pointing uniformly distributed load. The load results in compressive forces in the ring, according to Mariotte's formula for the calculation of stresses in a curved structure.

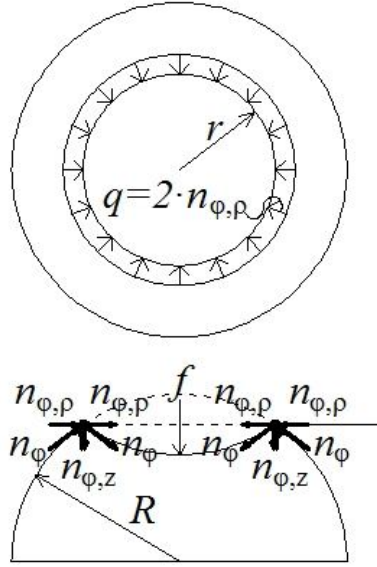


Figure 3.1.: Resultant forces acting to the circular buckling edge of a spherical shell in the case of concentrated force, applying membrane theory (except for the small neighbourhood of the loading point)

The horizontal meridional force component at the buckling edge is derived from the vertical balance of the inner region:

$$n_{\phi,\rho} = \frac{R-h}{r} \frac{f}{2r\pi} = \frac{f(R-h)}{2(2Rh-h^2)\pi}, \quad (3.1)$$

where R is the radius of the sphere, h is the half-deflection in the case of axisymmetric buckling shapes, $r = \sqrt{2Rh-h^2}$ is the radius of the buckling edge, f is the concentrated load. Equation (2.23), which describes the dependence between the concentrated load of the shell and its half-deflection, is used, thus the inward-pointing distributed load of the ring is:

$$q = 2n_{\phi,\rho} = \frac{f(R-h)}{(2Rh-h^2)\pi} = 3cEt^{5/2} \frac{\sqrt{2h}}{R} \frac{R-h}{2Rh-h^2} = 3\sqrt{2}cE \frac{t^{5/2}}{R^{3/2}} \frac{\sqrt{\bar{h}}(1-\bar{h})}{2\bar{h}-\bar{h}^2}. \quad (3.2)$$

The dimensionless variable $\bar{h} = h/R$ refers to the half-deflection in the case of axisymmetric buckling shapes.

The buckled shell is divided by the circular buckling edge into two parts. These spherical caps are connected to each other at the buckling edge. The caps are not able to perform inextensional deformations in this configuration if relative displacements between their edges are not allowed, see Section 2.1. Based on this fact, the deformations of the buckling edge are constrained by the neighbouring parts of the surface. In the analogy between the buckling edge and the compressed ring, this effect causes bedding for the ring, which is taken into consideration in the following calculations. Additionally, the buckling edge has nonzero width, which leads to the bending stiffness of the ring in the analogy.

The ring is assumed to be bedded by the neighbouring shell regions, which results in bedding stiffness. The bedding is assumed to act only in radial direction of the ring (i.e. springs are considered in radial direction). The bedding stiffness is regarded as zero for displacements in other directions and for rotations. The bedding stiffness k in radial direction of the ring is calculated using the theory of rotationally symmetric structures (*Márkus, 1967*):

$$k = \frac{Et}{R\sqrt{\frac{R}{t}\sqrt{3(1-\nu^2)}(2\bar{h}-\bar{h}^2)}}. \quad (3.3)$$

For the calculation of the critical load of the ring, the bending stiffness EI of the ring, thus its moment of inertia is needed. The buckling edge has nonzero width; its cross-section is regarded as a circular arc (Figure 3.2.). The arc length of the cross-section, according to *Pogorelov (Pogorelov, 1988)*, is $\sqrt{2Rt}$. The radius of the arc is calculated easily:

$$\rho = \frac{\sqrt{2Rt}}{\varphi}, \quad (3.4)$$

where ρ is the radius of the arc, φ is its central angle. The central angle of the arc is:

$$\varphi = 2\alpha = 2\arcsin(r/R) = 2\arcsin\left(\sqrt{2\bar{h}-\bar{h}^2}\right). \quad (3.5)$$

The moment of inertia of the circular arc about the vertical axis is:

$$\begin{aligned}
 I &= \frac{\rho_o^4 - \rho_i^4}{8} (\varphi - \sin \varphi) = \\
 &= \frac{\left(\frac{\sqrt{2Rt}}{2 \arcsin(\sqrt{2\bar{h} - \bar{h}^2})} + \frac{t}{2} \right)^4 - \left(\frac{\sqrt{2Rt}}{2 \arcsin(\sqrt{2\bar{h} - \bar{h}^2})} - \frac{t}{2} \right)^4}{8} \cdot \\
 &\cdot \left(2 \arcsin(\sqrt{2\bar{h} - \bar{h}^2}) - \sin \left(2 \arcsin(\sqrt{2\bar{h} - \bar{h}^2}) \right) \right), \tag{3.6}
 \end{aligned}$$

where ρ_o and ρ_i are the outer and inner radii of the arc, respectively.

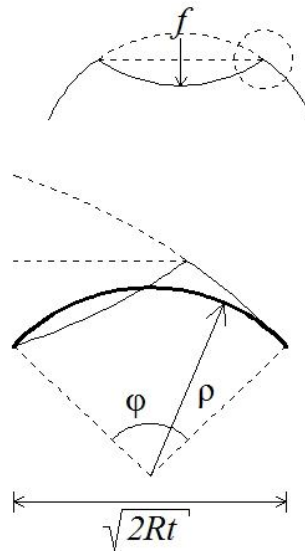


Figure 3.2.: The cross-section of the buckling edge, regarded as a circular arc (the difference between the isometric transformed shape (normal line) and the quasi-isometric transformed shape (bold line) can be examined, c. f. Figure 2.6.)

The above calculations were needed to determine the bending stiffness EI and the bedding stiffness k of the ring. Relative stiffness can be calculated from these two values, applied as a dimensionless parameter:

$$\bar{k} = \frac{EI}{kR^4}, \tag{3.7}$$

where R^4 in the denominator is chosen as a variable that remains unchanged during the loading process, while it provides \bar{k} to be dimensionless. It is obvious that the value of the dimensionless stiffness depends on dimensionless half-deflection \bar{h} , so it is not a constant value that can be assigned to a certain shell. The value \bar{k} permanently changes during the loading process. It is important to notice that \bar{k} is independent of Young's modulus.

There exists a critical load for the radially bedded ring for radial central loading. The critical load – which causes n -wave planar buckling of the ring – is given by the formula (Kollár, 1999):

$$q_{cr}^c = \frac{(n^2 - 1)^2}{n^2 - 2} \frac{EI}{r^3} + \frac{kr}{n^2 - 2}, \quad (3.8)$$

which can also be expressed by dimensionless parameters \bar{h} and \bar{k} :

$$q_{cr}^c = \frac{Et}{\sqrt{\frac{R}{t}} \sqrt{3(1-\nu^2)} (2\bar{h} - \bar{h}^2)} \left(\frac{(n^2 - 1)^2}{n^2 - 2} \frac{\bar{k}}{\left(\sqrt{2\bar{h} - \bar{h}^2}\right)^3} + \frac{\sqrt{2\bar{h} - \bar{h}^2}}{n^2 - 2} \right). \quad (3.9)$$

Formula (3.9) shows that the critical load of the ring for an n -wave planar buckling depends on \bar{h} and \bar{k} . It is obvious that there always exists an n integer for certain \bar{h} and \bar{k} , which concerns the minimum value of q_{cr}^c . As far as the buckling shape is axisymmetric (it means that the buckling edge is a circle), \bar{k} can be expressed with \bar{h} . This means that the above described model, based on the analogy between the buckling edge and a compressed ring, is able to predict the possible polygonal buckling shape, which evolves from the circle at a certain displacement. The model gives no result for the value of the displacement when this transformation of the shape occurs. The possible transformations between different polygonal shapes are also excluded from the model.

3.2. Results

Essentially, two types of shells were analysed in this model. The reason was the ability of comparison between different analytical models, experiments, and FE analyses. The first type of shells is the ping-pong ball, made of celluloid (Young's modulus: $E = 2400 \text{ N/mm}^2$, Poisson's ratio: $\nu = 0.3$, thickness: $t = 0.37 \text{ mm}$, radius: $R = 19.5 \text{ mm}$). The second type is the so-called Lénárt sphere (this was provided by mathematician István Lénárt), made of polyethylene (Young's modulus: $E = 2550 \text{ N/mm}^2$, Poisson's ratio: $\nu = 0.3$, thickness: $t = 0.42 \text{ mm}$, radius: $R = 102 \text{ mm}$). The exact geometry of these shells was measured; the above values are average values of the measured shells. The material constants (E, ν) are taken from the references (*Blaise et al, 2012, Ruan et al, 2006*) as average values. The radius-thickness ratios of the two types of shells differ by almost one order of magnitude: the ping-pong ball has a value of 52.70; the Lénárt sphere has a value of 242.86. The results of these shells are shown in Figures 3.3. and 3.4.

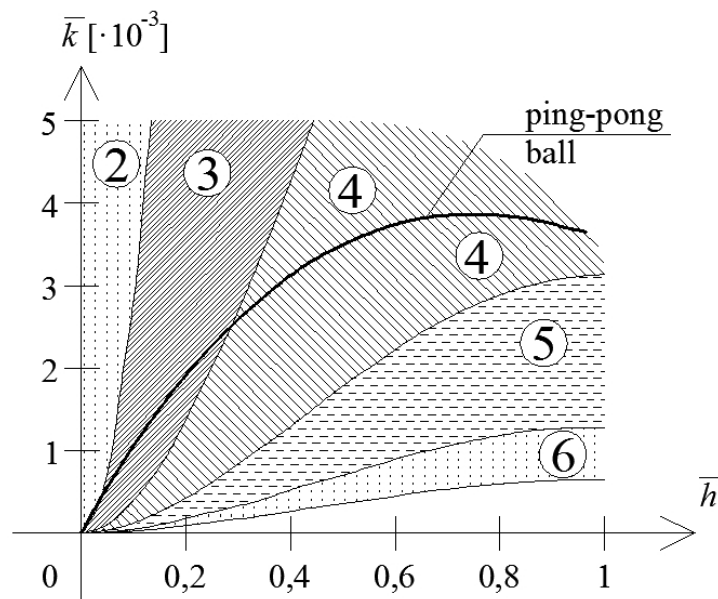


Figure 3.3.: Dimensionless stiffness-deflection diagram of the ping-pong ball (the behaviour of the circular buckling edge of the shell is characterised by the bold line, while the numbered zones indicate the possible number of sides of the buckling polygon that the circular buckling edge can transform to)

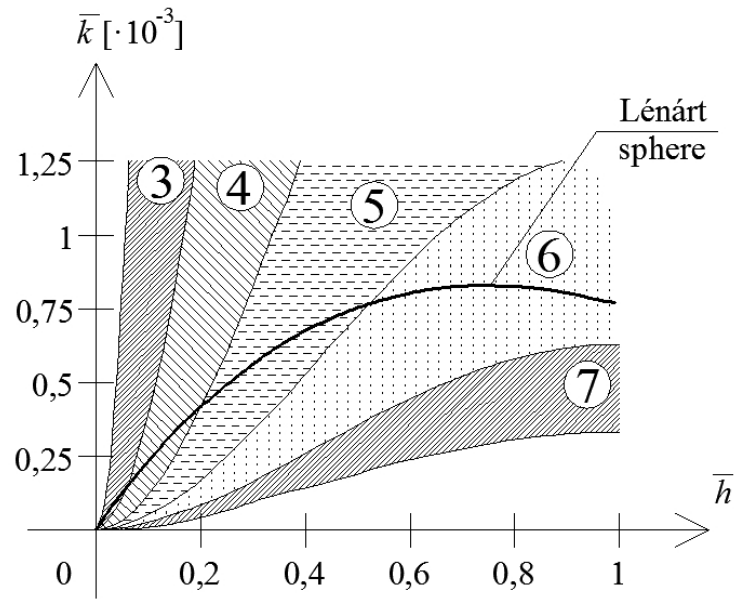


Figure 3.4.: Dimensionless stiffness-deflection diagram of the Lénárt sphere (the behaviour of the circular buckling edge of the shell is characterised by the bold line, while the numbered zones indicate the possible number of sides of the buckling polygon that the circular buckling edge can transform to)

The solid lines on diagrams show the dependence of dimensionless parameter \bar{k} of the buckling edge (modelled as a ring) on the dimensionless half-deflection \bar{h} . The zones on the diagrams indicate the n numbers of the waves of the buckling shape of the ring, corresponding to the lowest critical load. It is important to note that not all the buckling polygons (denoted by numbers in Figures 3.3. and 3.4.) appear during the buckling process. The diagrams show only the possibility of these polygonal buckling shapes.

The model gives no result for the value of the displacement when this transformation of the shape occurs. This value can be estimated based on experiments: it is approximately $0,15 \leq \bar{h} \leq 0,20$. Vaziri et al. (Vaziri-Mahadevan, 2008, Vaziri, 2009) place this value between 0,13 and 0,25 in the case of the ping-pong ball, and between 0,03 and 0,09 in the case of the Lénárt sphere, but the latter values are not verified by my experiments.

Figure 3.3. shows that in the case of the ping-pong ball, triangle is the possible shape in this interval of the dimensionless half-deflection (i.e. when $0,15 \leq \bar{h} \leq 0,20$). Figure 3.4. shows the case of the Lénárt-sphere: rectangle and pentagon are the possible shapes. It should be noted however, that the stiffness-deflection curves can be different

for different shells; there exists a considerable scatter in geometric and material properties in reality. So some deviation from the above mentioned numbers of sides of polygons can take place. The material constants (E , ν) are also taken from the references (*Blaise et al, 2012, Ruan et al, 2006*), which can cause additional differences. Furthermore, these calculations consider only the transition from the circle to a polygon, not the possible transition from a polygon to another polygon, which happened often for Lénárt spheres in experiments.

3.3. Summary and principal result 3

Axisymmetric buckling edge of spherical shells usually transforms into a polygonal edge with discrete symmetry of revolution if the loads are increased. There is a plausible analogy – based on engineering intuition – between the circular buckling edge of the spherical shell and a planar elastic bedded ring subjected to inward-pointing distributed load. Considering this analogy, one can relatively easily determine the possible polygonal buckling shapes that can evolve from the circle during buckling of a spherical shell with a certain radius-thickness ratio. The model considers only the point of transition from the circle to a regular polygon.

Principal result 3

(relevant publications: (*Vető-Sajtos, 2014, Vető-Sajtos, 2016a*))

I developed a qualitative model based on the analogy between the circular buckling edge of the point-loaded spherical shell and a planar elastic bedded ring subjected to inward-pointing distributed load. The analogy is verified by the physical behaviour of spherical shells. I showed that in the case of a certain spherical shell the possible number of sides of the buckling polygons can be determined by the model, which considers only the transition from the buckling shape with axisymmetry to the buckling shape with discrete symmetry of revolution. The results are supported by experiments in literature.

4. Analysis of buckling shapes with discrete symmetry of revolution

4.1. Description of buckling shapes with discrete symmetry of revolution

The buckling shape of spherical shells usually cannot be characterised by a circular edge. The edge can be similar to a polygon, according to experiments (Figure 1.9.). In most cases, circular buckling edge can be seen at small deflections, and polygonal buckling edge at larger deflections. The first case (that of circular buckling edge) can be described by Pogorelov's method, introduced in Chapter 2. The second case (the one of polygonal buckling edge) needs a new approach. Chapter 3 describes a qualitative model, based on the analogy between the circular buckling edge of the spherical shell and a planar elastic bedded ring subjected to inward-pointing distributed load, but it considers only the transition from the buckling shape with axisymmetry to the buckling shape with discrete symmetry of revolution. The aim of the present chapter is to construct a new model that is able to analyse the continuous transition between buckling shapes with axisymmetry and discrete symmetry of revolution.

The two most frequently used assumptions of the polygonal buckling edge are that this shape is planar and regular. In the dissertation these assumptions are adopted. The first one (that the buckling polygon is planar) is very close to reality, if one investigates a buckled shell. The second one (that the buckling polygon is regular) is usually also unquestionable, but sometimes the polygon seems to be a kind of non-regular one. These cases are not analysed in the dissertation; the topic needs further research.

The polygonal buckling edge, holding the assumptions written above, has a discrete symmetry of revolution. In reality, the edges of this kind of polygonal buckling shapes are slightly rounded (Figure 4.1.). If such a buckled shell surface is investigated, this effect is often neglected: our imagination completes the polygon out of the rounded formation. Most researchers do not take this effect into consideration, according to literature. My opinion is that the roundedness of the edges should be considered. In my

proposed model, presented in this chapter, buckling polygons can be rounded. The roundedness is controlled with a new parameter (b_2 , see Figures 4.1. and 4.2., description in Section 4.2.).

The connection between the buckling edge and the neighbouring parts of the shell surface is also a relevant issue. In my proposed model, there exists a so-called inner circle inside the buckling edge. Inside the inner circle, the buckled surface is considered as an inverted spherical surface, which is an isometric transformed shape of the original spherical surface. The diameter of the inner circle is less than or equal to the incircle of the buckling polygon. The peakedness of the buckling shape depends on the diameter of the inner circle, and it is controlled with a new parameter (b_1 , see Figures 4.1. and 4.2., description in Section 4.2.). Between the buckling polygon and the inner circle, the buckled surface is considered as a quasi-isometric transformed shape of the original shell surface. Outside the buckling polygon, the buckled surface is considered as a quasi-isometric transformed shape of the original shell surface, too. With these end in view, it can be stated that the shell surface is in a quasi-inextensional state. It means that on most of the shell surface the bending deformations are dominant, stretching deformations play an elemental role only at the buckling edge.

4.2. Analytical model

The proposed analytical model is able to handle not only axisymmetric buckling shapes, but buckling shapes with discrete symmetry of revolution, as well. The new model (*Vető-Sajtos, 2014, Vető-Sajtos, 2016a, Vető-Sajtos, 2016b*) is based on the methods published by Pogorelov (*Pogorelov, 1957, Pogorelov, 1988*), Audoly, Ben Amar, Pomeau (*Audoly-Pomeau, 2010, Ben Amar-Pomeau, 1997*), Lobkovsky (*Lobkovsky, 1996*), Pauchard, Rica (*Pauchard-Rica, 1998*), and Zhu et al. (*Zhu et al, 2002*). This model is a qualitative one: the principal aim for its construction was to understand the behaviour of spherical shells better in the post-buckling range. It is worth mentioning before the description of the model that the obtained results are in good agreement with experiments and FE analyses, concerning not only the number of sides of the buckling polygons, but also the load-deflection diagrams, see Chapter 5.

The buckling shape in the proposed model is assigned to a planar regular polygon, and the neighbouring parts of the buckled shell are joined to this figure by particular rules. The main point in the model is that the supposed buckling polygon has

the same perimeter as the original circle (i.e. the reference circle with radius r , see Figure 4.1.).

The parameters of the buckled shape are the following: h is the distance between the top of the original spherical shell and the plane of the buckling edge, n is the number of sides of the (regular) buckling polygon, b_1 is the peakedness of the centre of the buckled part (i.e. the ratio of the radius of the so-called inner circle (b_1m) and the incircle of the buckling polygon (m)), and b_2 is the roundedness of the buckling polygon (i.e. the ratio of the radius of the arc at the vertices of the polygon (b_2r) and the radius of the reference circle of the buckling shape (r)). These parameters exactly determine the geometry of the buckling edge. The top view and the section of the buckled spherical shell can be seen in Figure 4.1., and the effect of the variation of parameters b_1 and b_2 can be seen in Figure 4.2. Figure 4.1. shows that the total deflection of the shell is not necessarily equal to $2h$. According to the buckled shape of the shell inside the buckling edge, the value of the total deflection is $h + j + i$. The distance between the plane of the buckling polygon and the so-called inner circle is denoted by j , while the distance between the bottom of the buckled surface and the plane of the inner circle is denoted by i . It should be noted that axisymmetric buckling shapes can also be represented by the model ($b_1 = b_2 = 1$); in this special case $j + i = h$, and the total deflection is equal to $2h$. According to Figure 4.2., if $b_1 = 0$, the centre of the buckled part is totally peaked (the radius of the inner circle is zero), and if $b_1 = 1$, this part is totally spherical (the radius of the inner circle and the incircle of the buckling polygon are equal). If $b_2 = 0$, the buckling polygon has corners (sharp-edged, i.e. it is really a polygon), and if $b_2 = 1$, this figure is totally rounded (i.e. it is a circle). The other variables according to the buckling shape in Figure 4.1. are the following: r (4.1) is the radius of the reference circle of the buckling shape (it is the radius of the theoretical circular buckling edge belonging to half-deflection h), m (4.2) is the radius of the incircle, l (4.3) is the radius of the excircle of the buckling polygon. Expressions 4.4 and 4.7 determine deflection parameters i and j , respectively, and for the calculation of the latter one, the calculation of k (4.5) and g (4.6) are also needed.

$$r = \sqrt{2Rh - h^2} , \quad (4.1)$$

$$m = r \left(b_2 + \pi \frac{1 - b_2}{n \tan(\pi/n)} \right), \quad (4.2)$$

$$l = \frac{m - b_2 r}{\cos(\pi/n)} + b_2 r, \quad (4.3)$$

$$i = R \left(1 - \cos \left(\arcsin \left(\frac{b_1 m}{R} \right) \right) \right), \quad (4.4)$$

$$k = (1 - b_2) h, \quad (4.5)$$

$$g = \arcsin \left(\frac{R - h - k}{R} \right), \quad (4.6)$$

$$j = \sqrt{\left(R \left(\frac{\pi}{2} - g \right) - \sqrt{k^2 + (R \cos(g) - l)^2} - R \arcsin \left(\frac{b_1 m}{R} \right) \right)^2 - (l - b_1 m)^2}. \quad (4.7)$$

The above definition of variables gives the model the possibility of considering continuous transition between axisymmetric and polygonal shapes by parameters b_1 and b_2 , which are elements of the $[0;1]$ closed interval on the set of rational numbers. It is quite unusual to have a model which makes this transition possible. Almost all publications consider axisymmetric buckling shapes and shapes with discrete symmetry of revolution as separate phenomena. According to these models, the shell can change between these shapes by jumps. Experiments contradict this circumstance: usually the original axisymmetric buckling shape changes to a shape with discrete symmetry of revolution by a slow continuous transition. By taking this effect into account, the proposed model is closer to reality than the available models, found in literature.

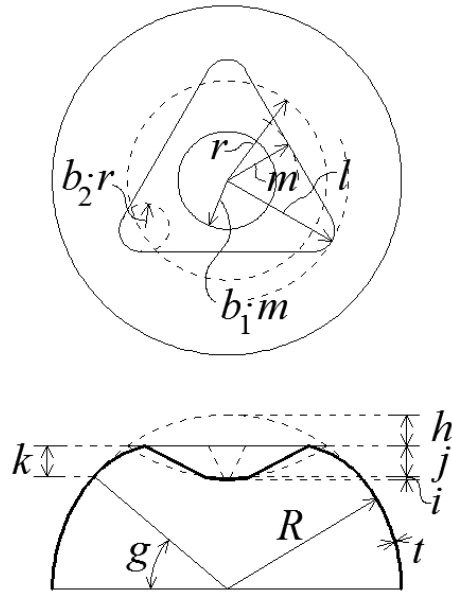


Figure 4.1.: Top view and section of buckling shape with discrete symmetry of revolution, as considered in the model (the variables belonging to the geometry of the buckled shell can be examined in the case of $n = 3$)

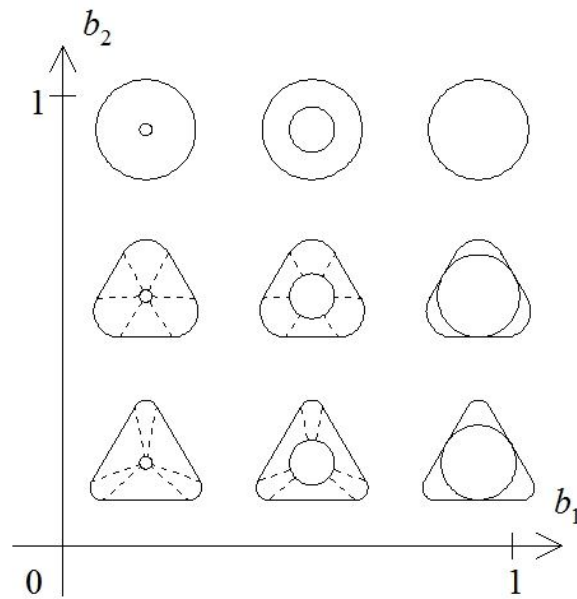


Figure 4.2.: Effect of the variation of geometric parameters b_1 and b_2

The equilibrium states of the buckled shell can be found by means of the energy method, as it can be done in the axisymmetric case, as well. Calculation of the strain energy of the buckled shell surface can be made according to the division of the surface illustrated by Figure 4.3. The strain energy of 8 different parts are considered: the bending energy on different parts of the surface, the stretching and bending energy

along the buckling edge, and the highly concentrated strain energy in the vertices. These parts are identified by Latin numbers.

The bending energy on parts *I*, *II*, and *III* of the surface are calculated as follows:

$$U = \frac{1}{2} \int_S \frac{Et^3}{12(1-\nu^2)} (\kappa_1^2 + \kappa_2^2 + 2\nu\kappa_1\kappa_2) dS, \quad (4.8)$$

where U is the strain energy on a certain part of the surface, E is Young's modulus, t is the thickness of the shell, ν is Poisson's ratio, κ_1 and κ_2 are the principal changes of curvature, and both terms of the expression are integrated over the surface S of the certain part.

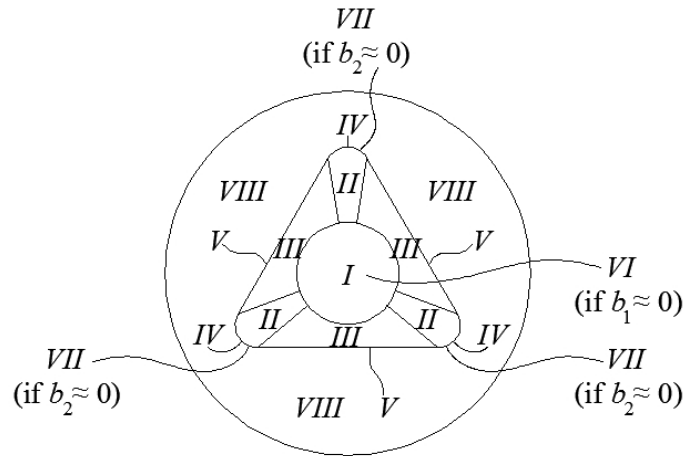


Figure 4.3.: Division of the buckled surface into zones in order to calculate the deformation energy for the model (top view of buckling shape with discrete symmetry of revolution, $n = 3$)

Surface part *I* is a mirror-reflected (inverted) spherical surface, part *II* is a kind of ellipsoidal surface (with a relatively large radius of curvature in the radial direction of the buckled shape), part *III* is also a kind of ellipsoidal surface (with a relatively small radius of curvature in the radial direction of the buckled shape). The principal changes of curvature on surface part *I*:

$$\kappa_{1,I} = \kappa_{2,I} = -\frac{2}{R}, \quad (4.9)$$

on surface part *II*:

$$\kappa_{1,II} = -\frac{b_1 m + b_2 r}{R^2 2 \cos\left(\arctan\left(\frac{l - b_1 m}{j}\right)\right)} - \frac{1}{R}, \quad (4.10)$$

$$\kappa_{2,II} = -\frac{2 \cos\left(\arctan\left(\frac{l - b_1 m}{j}\right)\right)}{b_1 m + b_2 r} - \frac{1}{R}, \quad (4.11)$$

and on surface part *III*:

$$\kappa_{1,III} = \frac{1}{\sqrt{((1 - b_1)m)^2 + j^2}} - \frac{1}{R}, \quad (4.12)$$

$$\kappa_{2,III} = \frac{\sqrt{((1 - b_1)m)^2 + j^2}}{R^2} - \frac{1}{R}. \quad (4.13)$$

The stretching and bending energy along buckling edges *IV* and *V* are calculated on the basis of the research of Pogorelov (*Pogorelov, 1988*), by an expression used by Zhu et al. (*Zhu et al, 2002*):

$$U = cEt^{2.5} \frac{\alpha^2 l_e}{R^{0.5}}, \quad (4.14)$$

where U is the strain energy of the edge, $c = 0.19$ is a dimensionless constant, α is the angle between the tangent planes of the surface parts that osculate to the edge, l_e is the length of the edge, R is the radius of the sphere.

Edge *IV* is the “corner” of the buckling polygon, with a radius of $b_2 r$, while edge *V* is straight. The length and angle corresponding to edge *IV*:

$$\alpha_{IV} = \arctan\left(\frac{j}{l - b_1 m}\right) + \arctan\left(\frac{k}{R \cos(g) - l}\right), \quad (4.15)$$

$$l_{e,IV} = \frac{2b_2 r \pi}{n}, \quad (4.16)$$

and to edge V :

$$\alpha_V = \arctan\left(\frac{j}{(1-b_1)m}\right) + \arctan\left(\frac{k}{R \cos(g) - m}\right), \quad (4.17)$$

$$l_{e,V} = 2(m - b_2 r) \tan(\pi/n). \quad (4.18)$$

The edges of the surface can sometimes transform into vertices, where additional strain energy has to be taken into account. These vertices cannot evolve without stretching of the surface, so they are not the result of isometric transformation. They are approximated by the so-called s-cones. The vertices that evolve by crumpling a planar surface are called d-cones, as a remark (*Audoly-Pomeau, 2010, Ben Amar-Pomeau, 1997*). The strain energy here is determined by approximate formulae, according to the above mentioned references. The places in the model where vertices can evolve are denoted by numbers VI and VII . The expression for the stretching energy is:

$$U = \frac{1}{2} \int_S \frac{Et}{(1-\nu^2)} (\varepsilon_1^2 + \varepsilon_2^2 + 2\nu\varepsilon_1\varepsilon_2) dS, \quad (4.19)$$

where ε_1 and ε_2 are the principal strains. Vertex VI evolves in the case of small values of b_1 , as it is shown by the expression for the principal strains:

$$\varepsilon_{1,VI} = \varepsilon_{2,VI} = \sqrt{\frac{t}{R} \frac{1/b_1 - 1}{2}}, \quad (4.20)$$

while vertex VII evolves in the case of small values of b_2 :

$$\varepsilon_{1,VII} = \varepsilon_{2,VII} = \sqrt{\frac{t}{R} \frac{1/b_2 - 1}{2}}. \quad (4.21)$$

The stretching energy (membrane strain energy) is also taken into consideration on the unbuckled parts, denoted by number *VIII*. Expression 4.19 is used to calculate the deformation energy, based on membrane theory, applying the following principal strains:

$$\varepsilon_{1,VIII} = -\frac{f}{Et} \frac{1+\nu}{2R\pi(r/R)^2}, \quad (4.22)$$

$$\varepsilon_{2,VIII} = \frac{f}{Et} \frac{1+\nu}{2R\pi(r/R)^2}. \quad (4.23)$$

The stretching energy on the buckled surface is generally not significant, but it has a governing role in edges and vertices, as it can be seen in the model of Pogorelov (*Pogorelov, 1988*). The work performed by the concentrated load can be calculated similarly to the axisymmetric case, see (2.13).

The implementation of the proposed model was carried out in MATLAB 7.11.0. The search for the equilibrium states of the shell was made by means of a built-in multi-variable constrained minimum seeking algorithm ('fminsearchbnd'). During the numerical calculations, the number of sides of the buckling polygon (n) was always kept unchanged, because this variable can only take integer numbers. This causes that there is no possibility in this model for the transition between shapes with different numbers of sides of buckling polygons. The transition can be realised through non-regular polygons (as it can be seen in experiments, see Section 5.1.), but this is not contained in the proposed model. The other parameters of the buckling shape (h , b_1 , and b_2) and the load intensity (f) were set in the range of physically reasonable domains.

Basically two types of shells were analysed in this model. The reason was the ability of comparison between different analytical models, experiments, and FE analyses. The first type of shells is the ping-pong ball (radius $R = 19.5$ mm), the second type is the Lénárt sphere ($R = 102$ mm), see Section 3.2.

4.3. Results

The load-deflection-roundedness diagram of the point-loaded ping-pong ball can be seen in Figure 4.4.; the load-deflection diagram and the roundedness-deflection

diagram can be seen in Figures 4.5. and 4.6., respectively (*Vető-Sajtos, 2016a, Vető-Sajtos, 2016b*). The load-deflection-roundedness diagram of the point-loaded Lénárt sphere can be seen in Figure 4.7.; the load-deflection diagram and the roundedness-deflection diagram can be seen in Figures 4.8. and 4.9., respectively (*Vető-Sajtos, 2016a, Vető-Sajtos, 2016b*).

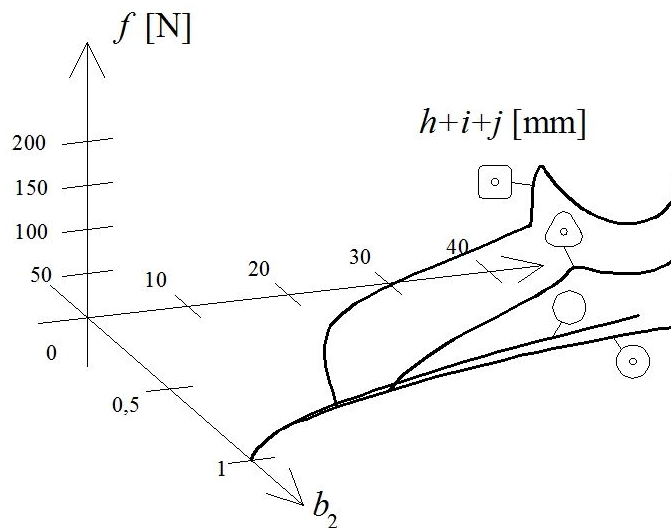


Figure 4.4.: Load-deflection-roundedness diagram of the ping-pong ball

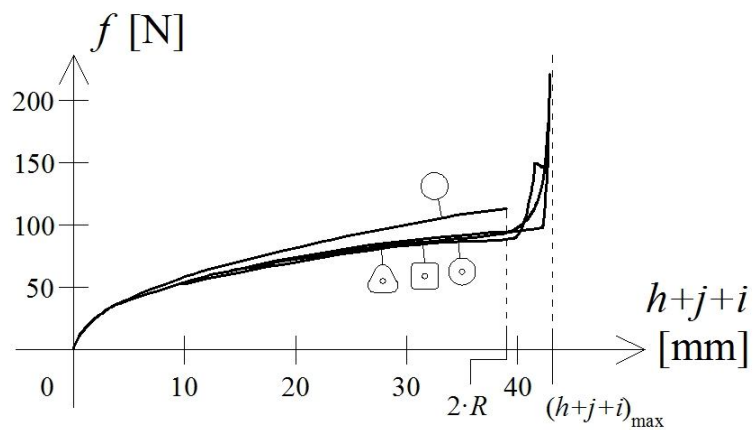


Figure 4.5.: Load-deflection diagram of the ping-pong ball

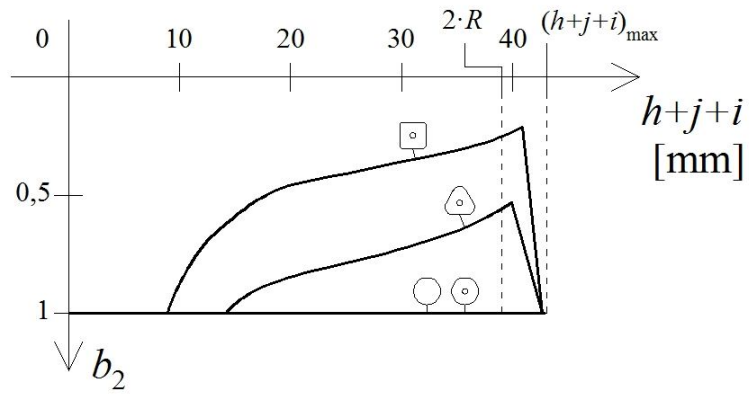


Figure 4.6.: Roundedness-deflection diagram of the ping-pong ball

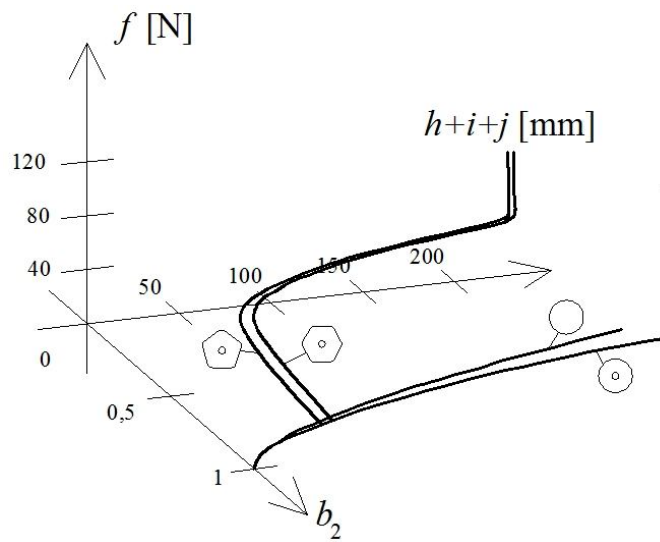


Figure 4.7.: Load-deflection-roundedness diagram of the Lénárt sphere

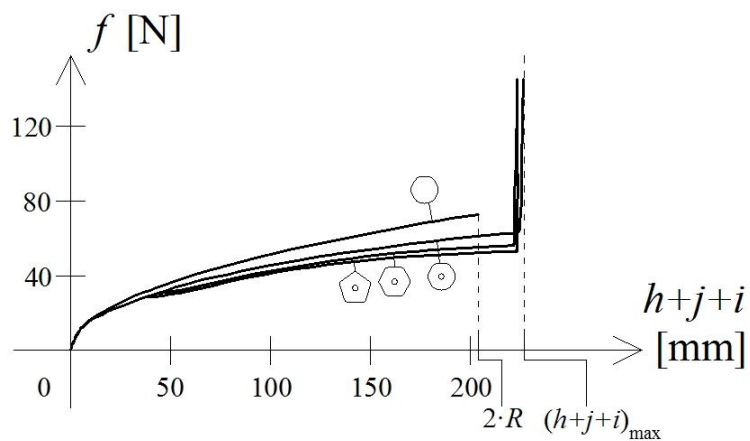


Figure 4.8.: Load-deflection diagram of the Lénárt sphere

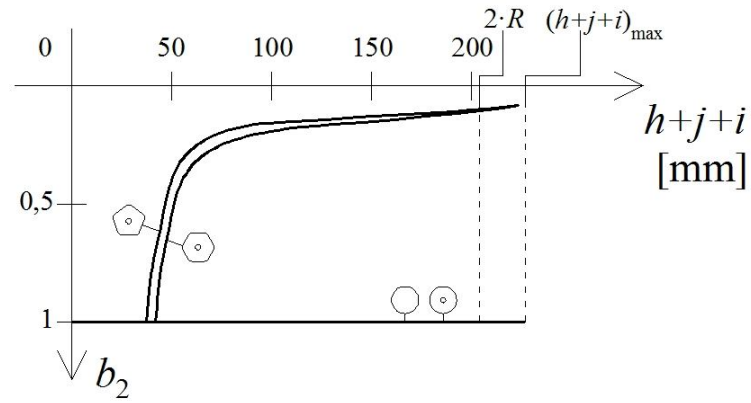


Figure 4.9.: Roundedness-deflection diagram of the Lénárt sphere

The proposed model is able to take buckling shapes with discrete symmetry of revolution into consideration, while Pogorelov’s model can only handle axisymmetric buckling shapes. The load-deflection diagrams (Figures 4.5. and 4.8.) show that the two models give the same solution for smaller deflections. In the case of larger deflections, however, a noticeable difference appears: the diagrams that belong to buckling shapes with discrete symmetry of revolution are located at lower load levels than the diagrams that belong to axisymmetric buckling shapes. This is the reason why “it is worth” for the shell choosing the polygonal buckling shape instead of the circular one.

The roundedness-deflection diagrams (Figures 4.6. and 4.9.) show the bifurcation of the equilibrium paths of buckling shapes with discrete symmetry of revolution from the equilibrium paths of axisymmetric buckling shapes. The complete development of buckling polygons happens beyond these branching points, in the case of larger deflections. Hence, the case of branching does not mean the sudden appearance of a certain polygon. Usually the polygonal buckling shape in the vicinity of the branching point shows no difference from the circle. The proposed model gives a relatively simple tool to examine the phenomenon of the transition between circular and polygonal buckling shapes. The model is unique in a sense that it handles the above mentioned transition of the shell as a continuous process instead of a sudden event, as most models do (Fitch, 1968, Vaziri-Mahadevan, 2008, Vaziri, 2009). As an exception, there exists an early model of Pogorelov (Pogorelov, 1963) which is able to handle buckling shapes with discrete symmetry of revolution. His model has a parameter that takes the roundedness of the buckling shape into consideration (but the peakedness of the centre of the buckled part is out of consideration in the model). Among his results

one can find a critical load for the appearance of the polygonal buckling shape, characterised by 3 waves:

$$f_{cr} = \frac{3\pi Et^3}{R}, \quad (4.24)$$

which gives a value of 58,76 N for the ping-pong ball. The load value that belongs to the bifurcation point of the triangle in the proposed model (approximately 62 N) shows relatively good agreement with this value. In the case of the Lénárt sphere the comparison can not be made, because in this case no triangle appears.

The load-deflection-roundedness diagrams (Figures 4.4. and 4.7.) show that there are more than one equilibrium paths for a certain shell. Note that these equilibrium paths correspond to regular polygons and circles as buckling shapes. A question arises here: which one is chosen by the shell? In the case of the ping-pong ball (Figure 4.4.), there are branches for circular, triangular and rectangular buckling shapes. There exists no other equilibrium path, according to the calculation. The paths of triangles and rectangles are very close to each other on the load-deflection diagram (Figure 4.5.), but relatively far from each other on the roundedness-deflection diagram (Figure 4.6.). The distance of the paths provides theoretically no possibility in this model for the shell to change the number of the sides of the buckling polygon. This means that once a polygon has appeared, it will not change its number of sides during the whole loading process. In the case of the Lénárt sphere (Figure 4.7.), there are branches for circular, pentagonal and hexagonal buckling shapes. There exists no other equilibrium path, according to the calculation. The paths of pentagons and hexagons are very close to each other both on the load-deflection diagram (Figure 4.8.) and the roundedness-deflection diagram (Figure 4.9.). The distance of the paths provides theoretically no possibility in this model for the shell to change the number of the sides of the buckling polygon. But in practice, taking the approximations and imperfections into account, these two branches can be considered as one, so the shell can almost randomly choose from these two configurations. These analytical results are verified in the chapter of experimental results (Chapter 5).

It is interesting to observe the peakedness-deflection diagrams (Figures 4.10. and 4.11.). In both cases a sudden decrease of peakedness takes place, before the branching of polygonal shapes occurs. It means that the buckling shape becomes peaked when the

deflection reaches a certain value, but the configuration remains axisymmetric. The buckling shape with discrete symmetry of revolution evolves from this axisymmetric peaked shape when the deflection is increased further. If the approximate values of peakedness of the ping-pong ball and the Lénárt sphere are compared, it can be stated that the latter one realises smaller b_1 values, i.e. the shape is more peaked in this case, as it is verified by experiments.

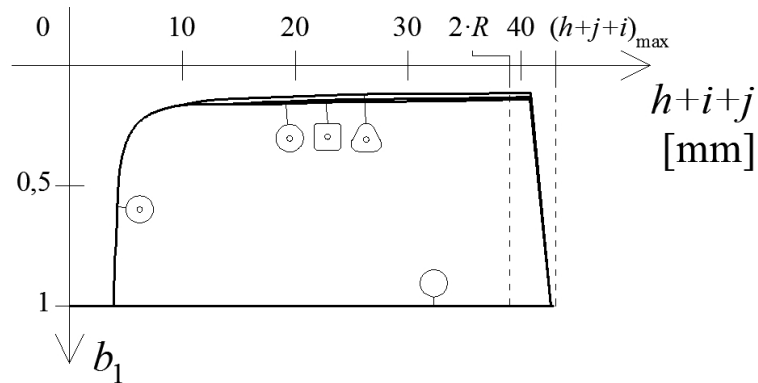


Figure 4.10.: Peakedness-deflection diagram of the ping-pong ball

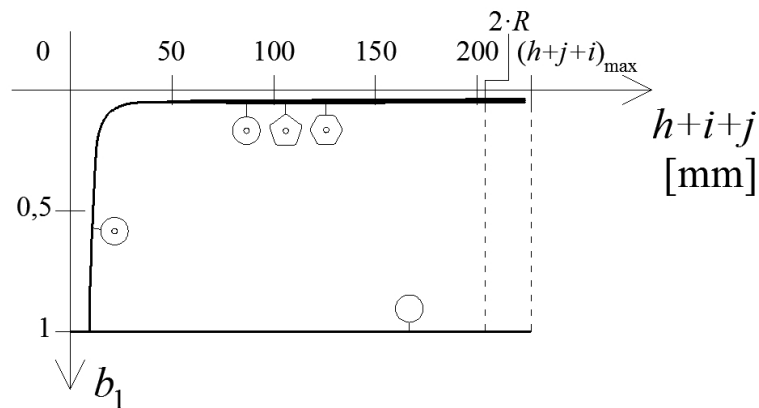


Figure 4.11.: Peakedness-deflection diagram of the Lénárt sphere

A parameter study has also been performed with the proposed model. 16 different shells were tested virtually. The radius-thickness ratio (R/t) varied between 50 and 2000. The radius-thickness ratio can be converted to the relative thickness parameter λ , which is widely used in literature, e. g. reference (Kollár-Dulácska, 1984):

$$\lambda = 2(3(1-\nu^2))^{1/4} (R/t)^{1/2}. \quad (4.25)$$

The analysed radius-thickness ratios (R/t) were the following: 50, 250, 1000, and 2000; the corresponding λ values were: 18.18, 40.65, 81.30, and 114.97. The numbers of the sides of the buckling polygons depend on relative thickness, as it can be seen in Figure 4.12. The shells with smaller λ (thus smaller R/t) exhibit polygons with smaller numbers of sides, compared to shells with larger λ (larger R/t). For the ping-pong ball λ is 18.42, while for the Lénárt sphere λ is 40.06.

Vaziri et al. (Vaziri-Mahadevan, 2008, Vaziri, 2009) state that the complete sequence of regular polygons (starting with triangle) appear during buckling, as deflection is increased. My results are different: only a few numbers of the sides of the buckling polygons can exist during the buckling process of a certain shell. Vaziri et al. also state that transformation between circular and polygonal buckling shape happens at a deflection value depending on relative thickness. This statement is verified by my results: in the case of shells with larger R/t ratios the buckling circles turn into polygons at smaller deflections, compared to the case of shells with smaller R/t ratios.

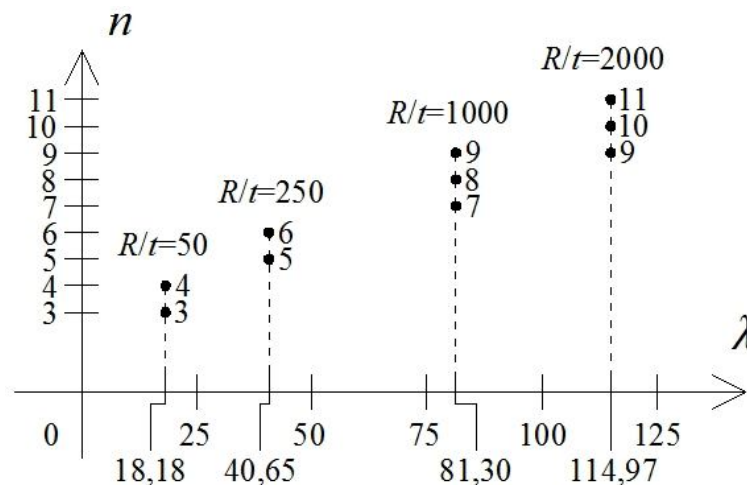


Figure 4.12.: Numbers of sides of buckling polygons, depending on the relative thickness parameter λ

The possible maximum deflections are also indicated in Figures 4.5., 4.6., 4.8., and 4.9. In the case of maximum deflection, the buckling edge is circular ($b_2 = 1$), having a radius of R , but the buckled part is totally peaked ($b_1 = 0$), i.e. a cone-like waved shape is assumed. This case is physically impossible if a complete sphere is considered (because the shell surface has intersection with oneself), but the value of the deflection has a theoretical significance:

$$(h + j + i)_{\max} = R \left(1 + \sqrt{\frac{\pi^2}{4} - 1} \right) \cong 2,21R, \quad (4.26)$$

which is 43.12 mm in the case of ping-pong ball, 225.26 in the case of Lénárt sphere. The shell never reaches this configuration because it generates infinitely large stresses. The possible maximum deflections ($2R$), according to Pogorelov's model, are also indicated in Figures 4.5., 4.6., 4.8., and 4.9.

4.4. Summary and principal results 4 (excluded result 4.3) and 5

An analytical model was developed, based on references (*Audoly-Pomeau, 2010, Ben Amar-Pomeau, 1997, Lobkovsky, 1996, Pauchard-Rica, 1998, Pogorelov, 1957, Pogorelov, 1988, Zhu et al, 2002*), in order to examine the buckling of spherical shells, assuming quasi-isometric transformed shapes as buckling shapes. The model, which was implemented in MATLAB, is able to handle not only axisymmetric shapes, but shapes with discrete symmetry of revolution, as well. Continuous transitions between these different buckling shapes can be taken into consideration in the model. The transition is achieved by the possibility of continuous change of roundedness and peakedness parameters corresponding to the geometry of the buckled surface. This is unique among the available models. The results of this relatively simple qualitative model give us a better insight into the post-buckling behaviour of spherical shells.

Principal result 4 (excluded result 4.3)

(relevant publications: (*Vető-Sajtos, 2014, Vető-Sajtos, 2016a, Vető-Sajtos, 2016b*))

Using quasi-isometric transformed shapes as buckling shapes, I developed an analytical energy function, which can be handled numerically to examine the post-buckling behaviour of spherical shells, considering shapes with axisymmetry and discrete symmetry of revolution as well.

4.1 The proposed model can be used to analyse the transition between buckling shapes with axisymmetry and discrete symmetry of revolution. The transition is achieved by the possibility of continuous change of roundedness and peakedness parameters corresponding to the geometry of the buckled surface.

4.2 It was shown by the proposed model that the load-deflection functions corresponding to buckling shapes with discrete symmetry of revolution bifurcate from the equilibrium path of the axisymmetric buckling shape. The buckling shapes with discrete symmetry of revolution correspond to lower energy levels compared to the axisymmetric buckling shape.

Principal result 5

(relevant publication: (*Vető-Sajtos, 2016a*))

I showed that in the case of buckling of spherical shells the possible number of sides of the buckling polygons increases monotonically with the radius-thickness ratio, according to numerical analyses.

5. Experiments and FE analyses

5.1. Experiments

Generally, experimental verification of analytical results is very important in research. This fact led me to perform the tests of real shells. The tests specimens were prepared in the testing laboratory of the Department of Mechanics, Materials and Structures at the Budapest University of Technology and Economics. The exact geometry of the tested shells was also measured here. The tests were carried out in the testing room of Senselektro Ltd.

15 ping-pong balls (radius $R = 19.5$ mm) and 4 Lénárt spheres ($R = 102$ mm) were tested in my experiments (*Vető-Sajtos, 2014, Vető-Sajtos, 2016a*), see Section 3.2. for details. The half-sphere test specimens were set up with clamped supports, made of gypsum plaster. The effect of the supports at higher deflections could not have totally been eliminated. The radius of the loading tip of the testing machine (where the concentrated load was introduced) was more than one order of magnitude smaller than the radius of the tested shells. The loading speed was 3 and 6 mm/min in the case of ping-pong balls and Lénárt spheres, respectively. The experiments covered a smaller range of deflections than the theoretical models. The reason could be found in the construction of the supports: deflection could not exceed the radius of the sphere.

A series of photos of the testing process can be seen in Appendix A for a ping-pong ball (test specimen No. 14), and in Appendix B for a Lénárt sphere (test specimen No. 3). The results are shown in Figures 5.1. and 5.2. These diagrams show not only the mean values, but also the minimum and maximum values of forces for a given deflection, to recognise the differences between the results of the tested shells. These differences can be explained by the scatter in the geometry and/or the material properties of the shells. Non-regular polygons also appeared in experiments, mainly in the case of Lénárt spheres. This can be an additional explanation for the scatter in the diagrams.

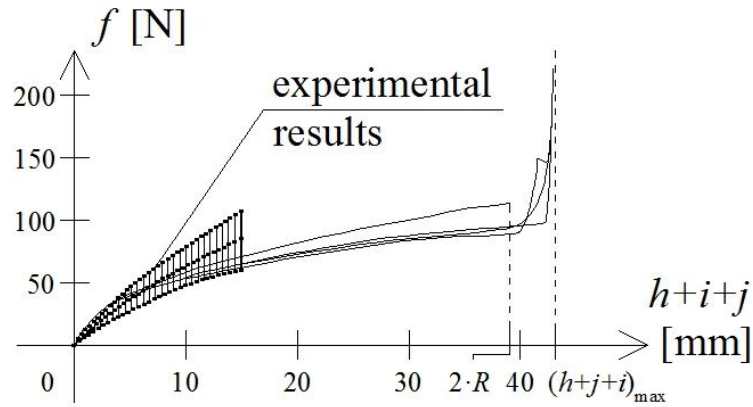


Figure 5.1.: Experimental results of ping-pong balls (the scatter between the results of 14 test specimens are denoted by the hatched zone), the load-deflection diagram shows the analytical results, as well

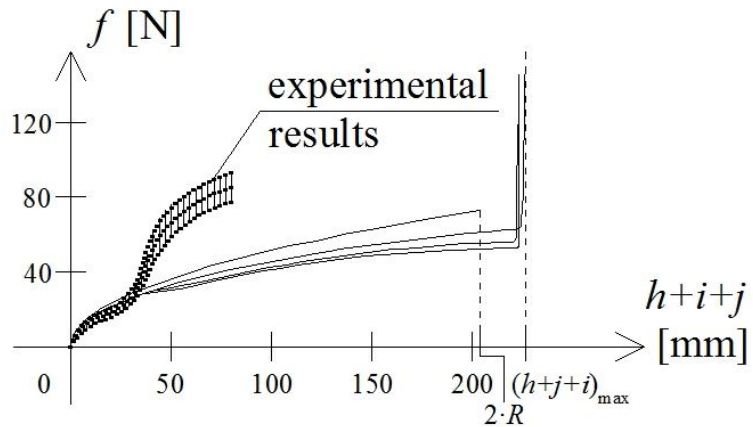


Figure 5.2.: Experimental results of Lénárt spheres (the scatter between the results of 4 test specimens are denoted by the hatched zone), the load-deflection diagram shows the analytical results, as well

11 ping-pong balls showed triangles as buckling shapes, only 3 showed rectangles. The remaining one ping-pong ball (out of 15) was broken during the test, so its result is neglected. Hence, the dominance of triangles is obvious. The geometry of the polygons in experiments was very close to regular polygons. The number of sides of the buckling polygon for a certain shell did not change at all during the whole loading process. The reason why the number of sides of a polygon did not change can be the relatively large distance between the curves on the roundedness-deflection diagram (Figure 4.6.) of the analytical model described in Chapter 4. It is also shown in Figure 4.6. that triangles and rectangles are the possible buckling shapes in the case of ping-pong balls. This is unambiguously verified by the experiments. The model of Chapter 3,

which is based on the analogy between the circular buckling edge of the spherical shell and a planar elastic ring subjected to inward-pointing distributed load, also supports the results.

The Lénárt spheres showed triangle, rectangles (2 times) and pentagon as buckling shapes after transformation from circle. The geometry of the polygons in experiments was sometimes far from regular polygons. Additionally, these shells showed sudden transitions between different polygons during the loading process, accompanied by loud noises. The reason for these transitions is the proximity of the curves on the roundedness-deflection diagram (Figure 4.9.) of the analytical model described in Chapter 4. It is also shown in Figure 4.9. that rectangles and pentagons are the possible buckling shapes in the case of Lénárt spheres. This is not perfectly verified by the experiments, because in one case of the experimental tests a triangle appeared, which is not predicted by the analytical model. The model of Chapter 3 also predicts rectangles and pentagons, as the model of Chapter 4. The reason for the difference between analytical and experimental results is still unknown for me, but there are many effects that can have influence on the buckling polygons, which are not taken into account in the analytical models. The non-regularity of buckling polygons, which appeared mainly in the case of Lénárt spheres, is the most probable reason.

It can be stated, based on my experiments that spherical shells subjected to concentrated load first buckle in an axisymmetric way, so the buckling edge is initially a circle. This shape continuously transforms into a polygon, when the load (and the deflection) is increased. This polygon can either conserve its number of sides or transform to other polygons. Many effects can influence the buckling shape (material inhomogeneities, effects of the support, loading speed, etc.), but it can be seen in experiments that, despite these effects, the shapes were not as various as they could have been. The analogy between the spherical shell and the compressed ring, described in Chapter 3, also gives a satisfactory explanation for the number of sides of buckling polygons in experiments.

The comparison among the load-deflection diagrams of experiments and the analytical model of Chapter 4 is also shown in Figures 5.1. and 5.2. In the case of ping-pong balls a good agreement can be seen, but in the case of Lénárt spheres, there is greater discrepancy: the experiments give larger loads to a certain displacement than my theoretical model and Pogorelov's model. The reason can be the effect of the change of the width of the buckling edge, which is excluded from my model. Another reason can

be the non-regularity of buckling polygons, which were not considered in the models, but appeared in experiments. The effect of the supports can also be seen in both cases, at relatively high deflections.

5.2. FE analyses

The buckling of point-loaded spherical shells was examined by means of finite element analyses. The ANSYS 12.1 software was used to verify the theoretical results of the ping-pong ball (*Vető-Sajtos, 2016a*). Unfortunately there was no possibility to examine the Lénárt sphere because of the limited accessibility to ANSYS. A half-sphere was modelled, and the supports of the shell along the bottom ring were clamped. Quadrilateral curved SHELL 281 elements with 8 nodes per element and 6 DOFs per node were used. Shear deformations are included in the element; however, normals to the centre plane remain straight after deformation. The mesh of the elements was made by a 6-degree-grid both in meridional and circumferential directions. The total number of shell elements was 840. A very small rigid plate was defined at the top of the shell, where the load was applied. Displacement-governed analyses were performed (displacement of the above mentioned small rigid plate was the governing displacement parameter).

A kind of fictive damping was used throughout the analyses, by means of a built-in algorithm ('stabilize'). The main point of this nonlinear stabilization technique is that artificial dampers are added to all the nodes in the system. To understand this technique, it is important to emphasize that in displacement-governed analyses in ANSYS, the step of the governing displacement parameter is called time step. When buckling occurs, relatively large displacements can occur over a small time step. As a result, pseudo velocities of the nodes become large and artificial dampers generate considerable resistive forces. The damping factor should be adjusted so that the total energy generated by the resistive forces through the displacements remains negligible.

The results can be seen in Figure 5.3. The ANSYS results and the results of the theoretical model of Chapter 4 show very good agreement. The experimental results slightly deviate from these curves at relatively high deflections, which can be attributed to the effect of the supports, which becomes considerable when the deflection increases, and could not have been totally eliminated.

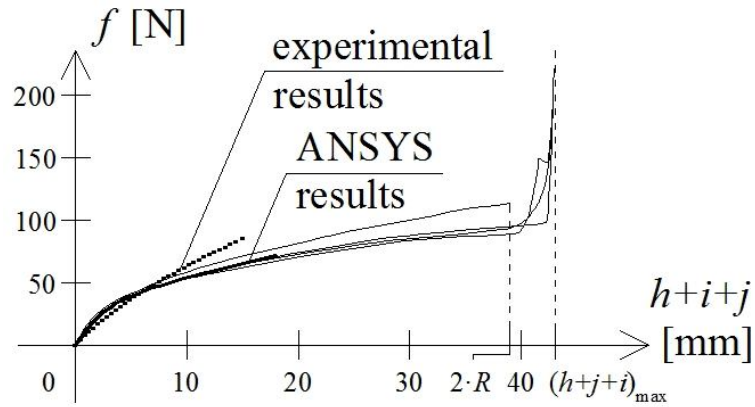


Figure 5.3.: Comparison between analytical, experimental and numerical (ANSYS) results (load-deflection diagram for the ping-pong ball)

5.3. Summary and principal result 4.3

Ping-pong balls and so-called Lénárt spheres were tested experimentally. Buckling of ping-pong balls was also examined by means of finite element analyses, using ANSYS. Experimental and FE results were compared to analytical results of the models in Chapters 3 and 4.

Principal result 4.3

(relevant publications: (Vető-Sajtos, 2014, Vető-Sajtos, 2016a))

According to the proposed model, the behaviour of spherical shells shows good agreement with the results of the performed experiments and finite element analyses, concerning the number of sides of the buckling polygons. The load-deflection diagrams of the performed experiments are in correspondence with the analytical results of the proposed model if the value of deflection does not exceed one-third of the radius of the sphere.

6. Summary and principal results

Large deflection analysis of thin elastic shells plays an essential role in mechanics and other fields of science. Generally, it is not easy to determine the connection between the load and the deflection of shells. Even now there exists a noticeable difference between theoretical and experimental results, which cannot be explained only by the imperfections, material nonlinearities and other effects that were not taken into account. Most differences can originate from the incompleteness of theoretical models.

Researchers used to consider axisymmetric buckling shapes for shells, although buckling shapes are usually non-axisymmetric (polygonal). It is stated by the researchers that the problem of buckling of spherical shells is not solved yet; therefore, the topic needs further investigation. There are several results available in the literature for non-axisymmetric (polygonal) buckling of point-loaded spherical shells. Although the same situation is being examined, the statements are sometimes different. The problem of spherical shell buckling is still current, with many substantial questions answered differently or not yet answered.

The goal of my research is to determine the buckling shape of point-loaded spherical shells. Additionally, the load-deflection function is also to be determined. To achieve these results, an analytical model was developed, which shows us the possible buckling shapes for spherical shells, and also the load-deflection diagrams connected to them. In the research, only regular polygons were taken into account among the possible non-axisymmetric shapes. These shapes have discrete symmetry of revolution. An approximate model – based on engineering intuition – was also developed, which only considers the point where the axisymmetric buckling shape transforms into a shape that has discrete symmetry of revolution. This shows which type of polygon is chosen by the shell at this point. Experimental and numerical (FE) results verify my models.

Many relevant and interesting statements are available about inextensional (isometric) deformations of surfaces in literature. The buckling shape of spherical shells can be approximated by an isometric transformed shape of the original surface. Surfaces

in reality have finite thickness. In the case of thin surface structures, typically locally inextensional (locally isometric) or quasi-inextensional (quasi-isometric) deformations occur. Based on simple considerations, it can be stated that there is no possibility for continuous inextensional deformations between buckling shapes with axisymmetry and discrete symmetry of revolution.

Axisymmetric buckling shapes are considered in many publications on the buckling of spherical shells. The buckled part of the surface can be assumed to be an inverted spherical surface. Based on this assumption, the load-deflection function can be determined. In the case of concentrated force, the results of Pogorelov are valid, while in the case of parallelly distributed load, new results are obtained. According to my solution, the load-deflection diagram has a minimum point, which belongs to the lower critical load of the shell. This critical load value shows good agreement with the critical load values found in literature.

Axisymmetric buckling edge of spherical shells usually transforms into a polygonal edge with discrete symmetry of revolution if the loads are increased. There is a plausible analogy – based on engineering intuition – between the circular buckling edge of the spherical shell and a planar elastic bedded ring subjected to inward-pointing distributed load. Considering this analogy, one can relatively easily determine the possible polygonal buckling shapes that can evolve from the circle during buckling of a spherical shell with a certain radius-thickness ratio. The model considers only the point of transition from the circle to a regular polygon.

An analytical model was developed in order to examine the buckling of spherical shells, assuming quasi-isometric transformed shapes as buckling shapes. The model, which was implemented in MATLAB, is able to handle not only axisymmetric buckling shapes, but buckling shapes with discrete symmetry of revolution, as well. Continuous transitions between these different shapes can be taken into consideration in the model. This is unique among the available models. Sudden transitions are considered between circular and polygonal buckling shapes by other researchers.

The load-deflection functions corresponding to buckling shapes with axisymmetry and discrete symmetry of revolution differ from each other. The difference among load-deflection diagrams of these different functions increase as the deflection of the shells increase. This demonstrates that consideration of buckling shapes with discrete symmetry of revolution is necessary. The proposed model is able to give a more

precise solution for the load-deflection function of spherical shells than the models of other researchers.

An additional result of the proposed model is that spherical shells with different radius and thickness show different polygonal buckling shapes. This simple model reveals that spherical shells with smaller radius-thickness ratios show smaller numbers of sides of buckling polygons, while spherical shells with larger radius-thickness ratios show larger numbers of sides of buckling polygons. As a summary of this part of the research, it can be clearly seen that the numbers of sides of the buckling polygons are determined by geometric parameters.

Generally, experimental verification of analytical results is very important in research. Ping-pong balls and so-called Lénárt spheres were tested in my experiments. Perfect agreement was found between the results of the performed experiments and the analytical results in the case of ping-pong balls. On the other hand, in the case of Lénárt spheres, the agreement between experimental and analytical results was found to be imperfect. The reason is still unknown, but there are many effects (material inhomogeneities, effects of the support, loading speed, etc.) that can have influence on buckling polygons, which are not taken into account in the analytical models. A probable reason can be the non-regularity of buckling polygons or the effect of the change of the width of the buckling edge, which were not considered in the models, but appeared in experiments. Buckling of point-loaded spherical shells was also examined by means of finite element analyses. The ANSYS results and the results of the theoretical model show very good agreement.

It is worth comparing my results with the results of some other researchers. Pauchard and Rica (*Pauchard-Rica, 1998*) state that polygonal configurations follow each other in an increasing order of the number of sides of the buckling polygon, as deflection is increased. The same can be read in the publications of Vaziri et al. (*Vaziri-Mahadevan, 2008, Vaziri, 2009*). My results cannot confirm these statements. In the case of ping-pong balls mostly triangles could be seen, and sometimes rectangles, but no transition between these shapes could be seen in experiments. In the case of Lénárt spheres, the order of the appearance of different polygons showed contrast to the results of the above mentioned researchers: sometimes a polygon with larger number of sides appeared sooner than another one with smaller number of sides. In the paper of Fitch (*Fitch, 1968*), the number of the sides of the polygon does not change during buckling: this is verified by my experiments in the case of ping-pong balls, but not in the case of

Lénárt spheres. It is also stated in this publication that the number of the sides of the polygon depends on the radius-thickness ratio, but the dependence is not the same as the one found by me. Bushnell and Penning (*Bushnell, 1967, Penning, 1966*) state that the number of sides of the buckling polygon can be 3, 4 and 5, usually in this order, but sometimes the experiments do not agree with these results.

As a summary, it can be stated that polygonal buckling of spherical shells is a complex and still unsolved problem, which cannot be examined with usual tools. Despite the simplifications that were made in my models, the results enlighten many interesting phenomena and answer some of the most important questions. It is evident that further research is needed in this field. My opinion is that the possible non-regularity of buckling polygons or the effect of the change of the width of the buckling edge, which are not included in my models, should be in the focus of research on this topic in the future.

Principal result 1

(relevant publication: (*Vető-Sajtos, 2009a*))

For spherical shells subjected to parallelly distributed load (which is distributed uniformly along the horizontal projection of the surface), considering the buckling shape as an axisymmetric quasi-isometric transformed shape of the shell, I determined analytically the load-deflection function in the post-buckling state and the lower critical load. The value of the lower critical load is in good agreement with analytical results obtained by different methods available in literature.

Principal result 2

(relevant publication: (*Vető-Sajtos, 2016b*))

I proved that two spherical shell caps (which can realise inextensional deformations), derived from the same sphere by intersection with a plane, are not able to perform inextensional deformations if their edges are joined in a way that the caps are located at the same side of the plane of the edges, except for the case of two half-spheres. Consequently, the axisymmetric buckling shape of spherical

shells cannot be transformed inextensionally into a buckling shape with discrete symmetry of revolution, if the buckled part is smaller than the half of the sphere.

Principal result 3

(relevant publications: (*Vető-Sajtos, 2014, Vető-Sajtos, 2016a*))

I developed a qualitative model based on the analogy between the circular buckling edge of the point-loaded spherical shell and a planar elastic bedded ring subjected to inward-pointing distributed load. The analogy is verified by the physical behaviour of spherical shells. I showed that in the case of a certain spherical shell the possible number of sides of the buckling polygons can be determined by the model, which considers only the transition from the buckling shape with axisymmetry to the buckling shape with discrete symmetry of revolution. The results are supported by experiments in literature.

Principal result 4

(relevant publications: (*Vető-Sajtos, 2014, Vető-Sajtos, 2016a, Vető-Sajtos, 2016b*))

Using quasi-isometric transformed shapes as buckling shapes, I developed an analytical energy function, which can be handled numerically to examine the post-buckling behaviour of spherical shells, considering shapes with axisymmetry and discrete symmetry of revolution as well.

4.1 The proposed model can be used to analyse the transition between buckling shapes with axisymmetry and discrete symmetry of revolution. The transition is achieved by the possibility of continuous change of roundedness and peakedness parameters corresponding to the geometry of the buckled surface.

4.2 It was shown by the proposed model that the load-deflection functions corresponding to buckling shapes with discrete symmetry of revolution bifurcate from the equilibrium path of the axisymmetric buckling shape. The buckling shapes with discrete symmetry of revolution correspond to lower energy levels compared to the axisymmetric buckling shape.

4.3 According to the proposed model, the behaviour of spherical shells shows good agreement with the results of the performed experiments and finite element analyses, concerning the number of sides of the buckling polygons. The

load-deflection diagrams of the performed experiments are in correspondence with the analytical results of the proposed model if the value of deflection does not exceed one-third of the radius of the sphere.

Principal result 5

(relevant publication: (*Vetř-Sajtos, 2016a*))

I showed that in the case of buckling of spherical shells the possible number of sides of the buckling polygons increases monotonically with the radius-thickness ratio, according to numerical analyses.

Acknowledgements

First of all, I would like to express my sincere gratitude to my supervisor, István Sajtos. He not only did his level best to provide me acceptable circumstances and helped me constantly in research, but also encouraged me several times.

I am also grateful to my colleague, Gábor Domokos. He helped me many times in my research from the very beginning. I gratefully thank my colleague, Endre Dulácska, the interest he showed for my research and the help he gave.

I am indebted to my colleagues András Sipos and Péter Várkonyi, and former colleague László Kollár, for their questions and help.

I am grateful to my colleague, Károly Juhász, for his help in experiments and in the use of ANSYS. I thank Ottó Sebestyén, Gábor Szabó, and the employees of Senselektro Ltd. the help in experiments. I thank István Lénárt for providing me the Lénárt spheres; and Géza Salát for letting me get acquainted with István Lénárt. I thank János Szenthe for spending time on teaching me differential geometry.

Last but not least I am really grateful to my family (my parents, my brother, and my sisters) for their endless support.

Publications connected to the principal results

- Vető, D., Sajtos, I. (2009a) Application of geometric method to determine the buckling load of spherical shells, *Pollack Periodica*, **4/2**, 123-134
- Vető, D., Sajtos, I. (2014) Geometriai módszer alkalmazása gömbhéjak horpadásának vizsgálatához (Application of geometric method to examine the buckling of spherical shells, in Hungarian), *Építés-Építészettudomány*, **42/3-4**, 241-259
- Vető, D., Sajtos, I. (2016a) Theoretical, numerical and experimental analysis of polygonal buckling shapes of spherical shells, *Journal of the IASS* – submitted for publication
- Vető, D., Sajtos, I. (2016b) Gömbhéjak poligonális horpadási alakjának vizsgálata (Examination of polygonal buckling shapes of spherical shells, in Hungarian), *Műszaki Szemle*, **68** – accepted for publication

Other publications in the subject of the research topic

- Vető, D., Sajtos, I. (2008) Application of geometric method to determine the buckling load of spherical shells, *In: Fourth International PhD, DLA Symposium, Pécs, 20-21.10.2008*, 61
- Vető, D., Sajtos, I. (2009b) Application of geometric method to determine the buckling load of spherical shells, *In: XXIII. microCAD International Scientific Conference, Miskolc, 19-20.03.2009*, 61-66
- Vető, D., Sajtos, I. (2009c) Investigation of buckling of spherical shells, *In: FUDoM 09, Finno-Ugric International Conference of Mechanics, Ráckeve, 23-29.08.2009*, 31-32
- Vető, D., Sajtos, I. (2011a) Geometriai módszer alkalmazása gömbhéjak horpadásának vizsgálatához (Application of geometric method to examine the buckling of spherical shells, in Hungarian), *In: XI. Magyar Mechanikai Konferencia, Miskolc, 29-31.08.2011*, 126
- Vető, D., Sajtos, I. (2011b) Geometriai módszer alkalmazása gömbhéjak horpadásának vizsgálatához (Application of geometric method to examine the buckling of spherical shells, in Hungarian), *In: XI. Magyar Mechanikai Konferencia, Miskolc, 29-31.08.2011*, 73, 1-6
- Vető, D., (2014a) Geometriai módszer alkalmazása gömbhéjak horpadásának vizsgálatához (Application of geometric method to examine the buckling of spherical shells, in Hungarian), *Magyar Építőipar*, 156-160
- Vető, D., Sajtos, I. (2015) Gömbhéjak poligonális horpadási alakjának elméleti és kísérleti vizsgálata (Theoretical and experimental analysis of the polygonal buckling shape of spherical shells, in Hungarian), *In: XII. Magyar Mechanikai Konferencia, Miskolc, 25-27.08.2015*, 121

Publications connected to the research topic in respects of the history of architecture

- Vető, D. (2010) For the centenary of Hungary's first reinforced concrete church in Rárósmulyad, *Periodica Polytechnica – Architecture*, **41/1**, 35-41
- Baku, E., Vető, D. (2012) A székesfehérvári Prohászka Ottokár Emléktemplom építéstörténete (History of the construction of Ottokár Prohászka Memorial Church in Székesfehérvár, in Hungarian), *In: XVI. Nemzetközi Építéstudományi Konferencia, Csíksomlyó, 07-10.06.2012*, 10-17
- Baku, E., Vető, D. (2013a) Centralized spaces in Hungarian church architecture between the world wars: historical and structural survey of the dome of Ottokár Prohászka Memorial Church, *Periodica Polytechnica – Civil Engineering*, **57/2**, 211-222
- Baku, E., Vető, D. (2013b) Vasbeton héjszerkezetek korai története (Beginning of the history of Hungarian reinforced concrete shell structures, in Hungarian), *In: 5. ÉTE Építésmenedzsment és Technológia Konferencia, Budapest, 22.11.2013.*, 1-6
- Vető, D. (2014b) Vasbeton kupolák kialakulása és fejlődése Magyarországon (Development of reinforced concrete domes in Hungary, in Hungarian), *Magyar Építőipar*, 103-107

Publications in the topic of structural engineering

- Sajtos, I., Hegyi, D., Sipos, A. Á., Vető, D., Merle, I., Orbán, I. (2010) *Falazott szerkezetek méretezése – Falazott szerkezetű épületek méretezésre földrengésre – Példatár* (Structural design of masonry structures – Structural design of masonry buildings for earthquake loads – Study aid, in Hungarian), Wienerberger Zrt. – study aid for structural engineers
- Fernezelyi, S., Vető, D. (ed.) (2013) *Acélszerkezetek tervezése építészeknek* (Structural design of steel structures for architects, in Hungarian) – university lecture notes

References

- Antman, S. (2005) *Nonlinear problems of elasticity*, Springer, New York
- Audoly, B. (2000) Élasticité et géométrie: de la rigidité des surfaces à la délamination en fil de telephone (in French), PhD thesis, École Normale Supérieure, Département de Physique, Paris, 2000
- Audoly, B., Pomeau, Y. (2010) *Elasticity and geometry*, Oxford University Press, Oxford
- Ben Amar, M., Pomeau, Y. (1997) Crumpled paper, *Proceedings of the Royal Society London A*, **453**, 729-755
- Blaise, A., André, S., Delobelle, P., Meshaka, Y., Cunat, C. (2012) Identification of the true elastic modulus of high density polyethylene from tensile tests using an appropriate reduced model of the elastoviscoplastic behavior, *arXiv:1206.4268v1* (date of access: 22.05.2016)
- Bronstein, I. N., Semendaiev, K. N., Musiol, G, Mühlig, H. (2002), *Matematikai kézikönyv* (Handbook of mathematics, in Hungarian), Typotex Kiadó, Budapest
- Bushnell, D. (1967) Bifurcation phenomena in spherical shells under concentrated and ring loads, *AIAA Journal*, **5/11**, 2034-2040
- Bushnell, D. (1985) *Computerized buckling analysis of shells*, Martinus Nijhoff Publishers, Dordrecht
- Croll, J. G. A. (1975) Towards simple estimates of shell buckling loads, *Der Stahlbau*, **9**, 283-285
- Csonka, P. (1981) *Héjszerkezetek* (Shell structures, in Hungarian), Akadémiai Kiadó, Budapest
- Dinno, K. S., Gill, S. S. (1974) A method for calculating the lower bound limit pressure for thick shells of revolution with specific reference to cylindrical vessels with torispherical ends, *International Journal of Mechanical Sciences*, **16/6**, 415-427
- Dulácska, E. (1987) Kupolahéjak horpadása (Buckling of dome shells, in Hungarian), *Építés-Építészettudomány*, **19/3-4**, 305-309
- El Naschie, M. S. (1990) *Stress, stability and chaos in structural engineering: an*

- energy approach*, McGraw-Hill Book Company, London
- Evkin, A. Yu. (2005) Large deflections of deep orthotropic shells under radial concentrated load: asymptotic solution, *International Journal of Solids and Structures*, **42**, 1173-1186
- Falco, C., Baccile, N., Titirici, M-M. (2011) Morphological and structural differences between glucose, cellulose and lignocellulosic biomass derived hydrothermal carbons, *Green Chemistry*, **13**, 3273-3281
- Feinberg, A. W., Feigel, A., Shevkoplyas, S. S., Sheehy, S., Whitesides, G. M., Parker, K. K. (2007) Muscular thin films for building actuators and powering devices, *Science*, **317/5483**, 1366-1370
- Fitch, J. R. (1968) The buckling and post-buckling behavior of spherical caps under concentrated load, *International Journal of Solids and Structures*, **4**, 421-446
- Flügge, W. (1973) *Stresses in shells*, Springer Verlag, Berlin, Heidelberg, New York
- Forgács, G. (1996) Fizika a biológiában (Physics in biology, in Hungarian), *Fizikai Szemle*, **3**, 95-101
- Galpin, B., Grolleau, V., Umiastowski, S., Rio, G., Mahéo, L. (2008) Design and application of an instrumented projectile for load measurements during impact, *International Journal of Crashworthiness*, **13/2**, 139-148
- Gould, P. L. (1988) *Analysis of shells and plates*, Springer, New York
- Grolleau, V., Galpin, B., Penin, A., Rio, G. (2008) Modeling the effect of forming history in impact simulations: evaluation of the effect of thickness change and strain hardening based on experiments, *International Journal of Crashworthiness*, **13/4**, 363-373
- Gupta, N. K., Mohamed Sheriff, N., Velmurugan, R. (2008) Experimental and theoretical studies on buckling of thin spherical shells under axial loads, *International Journal of Mechanical Sciences*, **50**, 422-432
- Hegedűs, I. (1998) *Héjszerkezetek* (Shell structures, in Hungarian), Műegyetemi Kiadó, Budapest
- Hutchinson, C. A. et al. (2016) Design and synthesis of a minimal bacterial genome, *Science*, **357/6280**, 1414/1-11
- Ivanova, J., Pastrone, F. (2002) *Geometric method for stability of non-linear elastic thin shells*, Kluwer Academic Publishers, Boston
- Knoche, S. (2014) Instabilities and shape analyses of elastic shells, PhD thesis, TU Dortmund, Faculty of Physics, Dortmund

- Knoche, S., Kierfeld, J. (2014) The secondary buckling transition: wrinkling of buckled spherical shells, *European Physical Journal E*, **37/7**, 1-21
- Kollár, L. (ed.) (1999) Structural stability in engineering practice, *E & FN Spon*, London, New York
- Kollár, L., Dulácska, E. (1984) *Buckling of shells for engineers*, Akadémiai Kiadó, Budapest
- Komura, S., Tamura, K., Kato, T. (2005) Buckling of spherical shells adhering onto a rigid substrate, *European Physical Journal E*, **18/3**, 343-358
- Lobkovsky, A. E. (1996) Structure of crumpled thin elastic membranes, PhD thesis, University of Chicago, Department of Physics, Chicago
- Márkus, Gy. (1967) *Theorie und Berechnung rotationssymmetrischer Bauwerke* (in German), Akadémiai Kiadó, Budapest
- Menyhárd, I. (1966) *Héjszerkezetek* (Shell structures, in Hungarian), Műszaki Könyvkiadó, Budapest
- Moulton, D. E., Goriely, A., Chirat, R. (2012) Mechanical growth and morphogenesis of seashells, *Journal of Theoretical Biology*, **311**, 69-79
- Niordson, F. I. (1985) *Shell theory*, Elsevier, Amsterdam
- Pauchard, L., Rica, S. (1998) Contact and compression of elastic spherical shells: the physics of a 'ping-pong' ball, *Philosophical Magazine B*, **78/2**, 225-233
- Penning, F. A. (1966) Nonaxisymmetric behavior of shallow shells loaded at the apex, *Journal of Applied Mechanics*, **33**, 699-700
- Pogorelov, A. V. (1957) *Die Verbiegung konvexer Flächen* (in German), Akademie-Verlag, Berlin
- Pogorelov, A. V. (1963) Stability of axially symmetric deformations of spherical shells under axially symmetric load (translation from Russian), NASA Contract TT F-8628, ST-SM-10050, Arlington, 1963
- Pogorelov, A. V. (1988) *Bendings of Surfaces and Stability of Shells* (translation from Russian), American Mathematical Society, Providence
- Prausnitz, M. R., Langer, R. (2008) Transdermal drug delivery, *Nature Biotechnology*, **26**, 1261-1268
- Quilliet, C., Zoldesi, C., Riera, C., Blandaren, A. van, Imhof, A. (2008) Anisotropic colloids through non-trivial buckling, *European Physical Journal E*, **27**, 13-20
- Ramm, E., Wall, W. A. (2004) Shell structures – a sensitive interrelation between physics and numerics, *International Journal for Numerical Methods in*

- Engineering*, **60**, 381-427
- Ruan, H. H., Gao, Z. Y., Yu, T. X. (2006) Crushing of thin-walled spheres and sphere arrays, *International Journal of Mechanical Sciences*, **48**, 117-133
- Shim, J., Perdigué, C., Chen, E. R., Bertoldi, K., and Reis, P. M. (2012) Buckling-induced encapsulation of structured elastic shells under pressure, *Proceedings of the National Academy of Sciences*, **109/16**, 5978-5983
- Singer, J., Arbocz, J., Weller, T. (2002) *Buckling experiments*, Wiley, New York
- Steele, C. R. (2000) Shell stability related to pattern formation in plants, *Journal of Applied Mechanics*, **67/2**, 237-247
- Tarnai, T. (1989) Buckling patterns of shells and spherical honeycomb structures, *Computers and Mathematics with Applications*, **17/4-6**, 639-652
- Thang, C. Q. (1989) A gömbhéj szimmetrikus horpadása (Symmetric buckling of spherical shells, in Hungarian), *Építés-Építészettudomány*, **21/1-2**, 95-108
- Tsapis, N. et al. (2005) Onset of buckling in drying droplets of colloidal suspensions, *Physical Review Letters*, **94**, 018302/1-4
- Vaziri, A., Mahadevan, L. (2008) Localized and extended deformations of elastic shells, *Proceedings of the National Academy of Sciences*, **105/23**, 7913-7918
- Vaziri, A. (2009) Mechanics of highly deformed elastic shells, *Thin-Walled Structures*, **47**, 692-700
- Vliegthart, G. A., Gompper, G. (2011) Compression, crumpling and collapse of spherical shells and capsules, *New Journal of Physics*, **13**, 1-24
- Wolmir, A. S. (1962) *Biegsame Platten und Schalen* (in German), VEB Verlag für Bauwesen, Berlin
- Wong, A. Y. K., Rautaharju, P. M. (1968) Stress distribution within the left ventricular wall approximated as a thick ellipsoidal shell, *American Heart Journal*, **75/5**, 649-662
- Zhu, E., Mandal, P., Calladine, C. R. (2002) Buckling of thin cylindrical shells: an attempt to resolve a paradox, *International Journal of Mechanical Sciences*, **44**, 1583-1601